



**HAL**  
open science

## Identification of the *Arabidopsis* calmodulin-dependent NAD<sup>+</sup> kinase that sustains the elicitor-induced oxidative burst

Elisa Dell'Aglio, Cécile Giustini, Alexandra Kraut, Yohann Couté, Alex Costa, Guillaume Decros, Yves Gibon, Christian Mazars, Michel Matringe, Giovanni Finazzi, et al.

### ► To cite this version:

Elisa Dell'Aglio, Cécile Giustini, Alexandra Kraut, Yohann Couté, Alex Costa, et al.. Identification of the *Arabidopsis* calmodulin-dependent NAD<sup>+</sup> kinase that sustains the elicitor-induced oxidative burst. *Plant Physiology*, 2019, 181 (4), pp.1449-1458. 10.1104/pp.19.00912 . hal-02361156

**HAL Id: hal-02361156**

**<https://hal.science/hal-02361156>**

Submitted on 13 Nov 2019

**HAL** is a multi-disciplinary open access archive for the deposit and dissemination of scientific research documents, whether they are published or not. The documents may come from teaching and research institutions in France or abroad, or from public or private research centers.

L'archive ouverte pluridisciplinaire **HAL**, est destinée au dépôt et à la diffusion de documents scientifiques de niveau recherche, publiés ou non, émanant des établissements d'enseignement et de recherche français ou étrangers, des laboratoires publics ou privés.

1 **The Arabidopsis Calmodulin-dependent NAD<sup>+</sup> kinase sustaining the elicitor-induced oxidative**  
2 **burst**

3 Elisa Dell'Aglio<sup>a,b</sup>, Cécile Giustini<sup>a</sup>, Alexandra Kraut<sup>c</sup>, Yohann Couté<sup>c</sup>, Alex Costa<sup>d</sup>, Guillaume Decros<sup>e</sup>,  
4 Yves Gibon<sup>e,f</sup>, Christian Mazars<sup>g</sup>, Michel Matringe<sup>a</sup>, Giovanni Finazzi<sup>a</sup>, Gilles Curien<sup>a\*</sup>

5 <sup>a</sup> Univ. Grenoble Alpes, CNRS, CEA, INRA, BIG-LPCV, 38000 Grenoble, France

6 <sup>b</sup> Department of Botany and Plant Biology, University of Geneva, 1211 Geneva, Switzerland

7 <sup>c</sup> Univ. Grenoble Alpes, CEA, INSERM, BIG-EdyP, 38000 Grenoble, France

8 <sup>d</sup> Department of Biosciences, University of Milan, 20133 Milan, Italy

9 <sup>e</sup> UMR1332 BFP, INRA, Univ. Bordeaux, Villenave d'Ornon, France

10 <sup>f</sup> MetaboHUB, Bordeaux, Villenave d'Ornon, France

11 <sup>g</sup> Laboratoire de Recherche en Sciences Végétales, Université de Toulouse, CNRS, UPS, 24, Chemin  
12 de Borde-Rouge, Auzeville, BP 42617, 31326 Castanet-Tolosan, France.

13 \* To whom correspondence may be addressed. E-mail: gilles.curien@cea.fr

14

15 Running title: Plant calmodulin-dependent NAD<sup>+</sup> kinase

16

17 **Abstract**

18 NADP(H) is an essential cofactor of multiple metabolic processes in all living organisms. In plants,  
19 NADP(H) is required as the substrate of Ca<sup>2+</sup>-dependent NADPH oxidases which catalyze a reactive  
20 oxygen species burst in response to various stimuli. While NADP<sup>+</sup> production in plants has long been  
21 known to involve a Calmodulin and Calcium (CaM)/Ca<sup>2+</sup>- dependent NAD<sup>+</sup> kinase, the nature of the  
22 enzyme catalyzing this activity has remained enigmatic, as well as its role in plant physiology. Here,  
23 thanks to a combination of proteomics, biochemistry, molecular biology and *in vivo* studies, we have  
24 identified an Arabidopsis protein that catalyzes NADP<sup>+</sup> production exclusively in the presence of  
25 CaM/Ca<sup>2+</sup>. This new enzyme (NADKc) has a CaM-binding peptide located in its N-terminal region and  
26 displays peculiar biochemical properties as well as different domain organization compared to known  
27 plant NAD<sup>+</sup> kinases. In response to a pathogen elicitor, activity of NADKc, which is associated with the  
28 mitochondrial periphery, contributes to an increase in the cellular NADP<sup>+</sup> concentration and to the  
29 amplification of the elicitor-induced oxidative burst. Based on a phylogenetic analysis and enzymatic  
30 assays, we propose that the CaM/Ca<sup>2+</sup>-dependent NAD<sup>+</sup> kinase activity found in photosynthetic

- 1 organisms is carried out by NADKc-related proteins. Thus, NADKc represents the missing link between
- 2  $\text{Ca}^{2+}$  signalling, metabolism and the oxidative burst.
- 3 **Keywords:**  $\text{NAD}^+$  kinase, Calmodulin, Calcium,  $\text{NADP}^+$ , zeta toxin, flagellin22, *Arabidopsis thaliana*.

## 1 **Introduction**

2 As sessile organisms, plants have evolved mechanisms to react quickly to stress conditions, such as  
3 changes in temperature, salinity or pathogen attacks. A common response to stress is a cytosolic calcium  
4 ( $\text{Ca}^{2+}$ ) influx followed by an apoplastic burst of Reactive Oxygen Species, or ROS burst (Grant et al.,  
5 2000). This ROS burst is generated by plasma membrane NADPH oxidases known as RBOH (for  
6 Respiratory Burst Oxidase Homologs, Torres and Dangl, 2005) and in turn regulates adaptation  
7 mechanisms such as gene expression, epigenetic changes and long-distance signal transduction  
8 (Liebthal and Dietz, 2017; Choi et al., 2017; Chapman et al., 2019). RBOH oxidase activity is dependent  
9 on  $\text{Ca}^{2+}$  binding to their EF-hand domains and is stimulated by phosphorylation by  $\text{Ca}^{2+}$ -dependent  
10 Protein Kinases (Dubiella et al., 2013) as well as CIPK/CBL complexes (Calcineurin B-Like Protein -  
11 CBL-Interacting Protein Kinase, Drerup *et al.*, 2013).

12 A rapid increase in the NADP(H) pool size was observed in response to plant treatment with a pathogen  
13 elicitor (Harding et al., 1997; Pugin et al., 1997) and may be required to sustain the ROS burst by fuelling  
14 RBOH proteins. Since most (~70-90%) of plant  $\text{NAD}^+$  kinase activity is dependent on binding  
15 Calmodulin (CaM) in its  $\text{Ca}^{2+}$ -loaded conformation (Anderson and Cormier, 1978) it was proposed  
16 (Harding et al., 1997) that the protein responsible for this activity may also be stimulated by the elicitor-  
17 induced  $\text{Ca}^{2+}$  influx.  $\text{NADP}^+$  produced by this enzyme may then be converted to NADPH (the substrate  
18 of RBOH proteins) by NADP-isocitrate dehydrogenase (Mhamdi et al., 2010) or by the reducing branch  
19 of the oxidative pentose phosphate pathway (Pugin et al., 1997; Scharte et al., 2009).

20 Several studies have described the CaM/ $\text{Ca}^{2+}$ -dependent  $\text{NAD}^+$  kinase activity in plants using partially  
21 purified enzymatic preparations from plant tissues. These studies allowed to find this protein activity in  
22 a wide variety of plant species (Dieter and Marmé, 1984; Delumeau et al., 2000; Turner et al, 2004),  
23 and to characterize its kinetic parameters (Delumeau et al., 2000; Turner et al., 2004) as well as its  
24 preferences for specific CaM and CaM-like isoforms (Turner et al., 2004). However, the protein  
25 responsible for CaM/ $\text{Ca}^{2+}$ -dependent  $\text{NAD}^+$  kinase activity has not been identified. In particular, among  
26 the three Arabidopsis  $\text{NAD}^+$  kinases identified to date, the plastidial NADK2 was shown to bind CaM  
27 *in vitro* in a  $\text{Ca}^{2+}$ -dependent way (Dell'Aglio et al., 2013a; Turner et al., 2004), but its activity does not

1 require CaM binding (Turner et al., 2004). Thus, this lack of knowledge of the identity of the plant CaM-  
2 dependent NAD<sup>+</sup> kinase has prevented a thorough characterization of its role in plant physiology, and  
3 in particular in the production of the stress-induced ROS burst.

4 Here, we report the characterization of an *A. thaliana* CaM/Ca<sup>2+</sup>-dependent NAD<sup>+</sup> kinase that displays  
5 all the properties of the elusive enzyme. We show that this NAD<sup>+</sup> kinase, which we named NADKc (for  
6 NAD kinase-CaM dependent), is associated with mitochondrial periphery and is involved in sustaining  
7 the ROS burst induced by the bacterial elicitor flagellin22.

## 8 **Results and discussion**

### 9 **NADKc is a new CaM/Ca<sup>2+</sup>-dependent NAD<sup>+</sup> kinase**

10 We obtained an Arabidopsis protein extract enriched in CaM/Ca<sup>2+</sup>-dependent NAD<sup>+</sup> kinase activity by  
11 a four-step purification procedure described in Supplemental Material and Methods. The last step  
12 consisted in binding the protein on a CaM-charged matrix in the presence of Ca<sup>2+</sup> and its subsequent  
13 release with an excess of the Ca<sup>2+</sup> chelator EGTA (Fig. S1). We then used mass spectrometry-based  
14 proteomics to identify proteins that were enriched in the EGTA elution compared to the Ca<sup>2+</sup>-containing  
15 washing steps (Supplemental Table S1). We reasoned that putative CaM/Ca<sup>2+</sup>-dependent NAD<sup>+</sup> kinases  
16 should display the following characteristics: *i*) have a molecular weight between 50 and 65 kDa, to  
17 respect the size range previously calculated by Delumeau et al., 2000; *ii*) be annotated as ATP-binding  
18 proteins (but not as a protein kinase), since it is known that plant CaM-activated NAD kinase uses ATP  
19 as a substrate (Anderson and Cormier, 1978); *iii*) contain a predicted CaM-binding site (following the  
20 guidelines of Rhoads and Friedberg, 1997) and *iv*) have no previously assigned enzymatic activity. Our  
21 analysis revealed only one protein – encoded by the At1g04280 gene – that fulfilled all these criteria.

22 To confirm its CaM/Ca<sup>2+</sup>-dependent NAD<sup>+</sup> kinase activity, we expressed the full-length recombinant  
23 protein coded by At1g04280 in *E. coli* with an N-terminal His-tag. We compared the NAD<sup>+</sup> kinase  
24 activity of two *E. coli* extracts: one obtained from an At1g04280-expressing strain and the second from  
25 a strain containing an empty vector. As shown in Fig. 1A, no NAD<sup>+</sup> kinase activity (which in our test  
26 was detected as an increase of absorbance at 340 nm) was detected in the *E. coli* strain containing the

1 empty vector, not even after the addition of an excess of  $\text{Ca}^{2+}$  and of *A. thaliana* Calmodulin 1 (AtCaM1).  
2 In contrast, addition of the At1g04280-expressing *E. coli* extract to the same reaction mixture  
3 immediately revealed  $\text{NAD}^+$  kinase activity.

4 Activity measurements with a partially purified At1g04280 enzyme confirmed the lack of  $\text{NAD}^+$  kinase  
5 activity in the absence of AtCaM1/ $\text{Ca}^{2+}$  and its appearance, within seconds, upon addition of both  
6 AtCaM1 and  $\text{Ca}^{2+}$ . This  $\text{NAD}^+$  kinase activity was suppressed by EGTA and restored by the addition of  
7 an excess of  $\text{Ca}^{2+}$ , showing that the CaM/ $\text{Ca}^{2+}$ -dependent enzyme activation is an all-or-none, reversible  
8 process (Fig. 1B). In contrast, while a CaM/ $\text{Ca}^{2+}$ -dependent  $\text{NAD}^+$  kinases have also been described in  
9 invertebrates, animal  $\text{NAD}^+$  kinase activity is only slightly increased by CaM/ $\text{Ca}^{2+}$  addition. For  
10 example, CaM induces a 3.5-fold increase of the NADK-2 activity of the sea urchin *Strongylocentrotus*  
11 *purpuratus* (Love et al., 2015).

12 Based on these results, we identified the At1g04280 gene product as the long-sought CaM/ $\text{Ca}^{2+}$ -  
13 dependent  $\text{NAD}^+$  kinase enzyme previously found in several plant species (Anderson and Cormier,  
14 1978, Delumeau et al., 1998, Turner et al., 2004) and named it *A. thaliana* “NADKc” for “NAD kinase-  
15 CaM dependent”.

### 16 **AtNADKc peculiar features in primary sequence and enzyme activity**

17 The primary sequence of NADKc (Fig. 1C) contains: *i*) an N-terminal region predicted to contain a  
18 transmembrane helix (amino acids: 1-45); *ii*) a domain of unknown function (amino acids 46-225) that  
19 includes a conserved putative CaM-Binding Site (CBS, Fig S2A); and *iii*) a C-terminal kinase domain  
20 (amino acids 226-340) similar to bacterial type II zeta-toxin domains (Khoo et al., 2007), which is  
21 predicted to contain a conserved P-loop for ATP binding (Walker A motif, WM, amino acids: 236-250,  
22 Fig S2B). Interestingly, these features are not shared with all other  $\text{NAD}^+$  kinases known to date, from  
23 bacteria, plants and animals (Fig. 1C, Kawai et al, 2001; Turner et al., 2004, Chai et al., 2006; Love et  
24 al., 2015).

25 To optimize NADKc expression levels in *E. coli* and improve the solubility of the protein, we removed  
26 the first 38 residues constituting the predicted transmembrane helix. The shorter version, 6HIS-

1  $\Delta 38\text{NADKc}$  was partially purified by Ni-NTA affinity chromatography (Fig. S3, lane 3). Activity assays  
2 with saturating AtCaM1/ $\text{Ca}^{2+}$  concentrations revealed the  $\text{NAD}^+$  kinase activity of NADKc to be  
3 specific toward  $\text{NAD}^+$ , as no activity could be detected with NADH or deamido- $\text{NAD}^+$  (NAAD) (Table  
4 1). Like most P-loop-containing kinases (Das et al., 2013), the enzyme displayed broad specificity for  
5 the phosphoryl donor, as ATP, CTP, GTP and UTP could be used indifferently and produced similar  
6 efficiencies (Table 1). The enzyme catalytic constant with CTP or ATP was close to  $40 \text{ s}^{-1}$  in the presence  
7 of  $\text{Ca}^{2+}$  and AtCaM1, *i.e.* about 10-fold higher than that reported for plant CaM/ $\text{Ca}^{2+}$ -independent  $\text{NAD}^+$   
8 kinases and other  $\text{NAD}^+$  kinases from bacteria and animals ( $0.5\text{-}7 \text{ s}^{-1}$ , (Kawai et al., 2001; Chai et al.,  
9 2006; Love et al., 2015; Turner et al., 2004)).

10 To characterize the interaction of NADKc with CaM, we further purified the recombinant enzyme by  
11 urea denaturation and rapid dilution (see Supplemental Material & Methods). The refolded protein (Fig  
12 S3, lanes 4-5) produced a single band on an SDS-PAGE gel and had an increased catalytic constant ( $70$   
13  $\text{ s}^{-1}$ ) compared to the partially purified enzyme ( $40 \text{ s}^{-1}$ , Table 1) and high affinity for CaM ( $k_d = 0.6\text{-}1 \text{ nM}$ ,  
14 Fig. 1D), similar to the value of  $0.4 \text{ nM}$  reported for the tomato CaM-dependent  $\text{NAD}^+$  kinase  
15 (Delumeau et al., 2000).

16 In conclusion, compared to all other  $\text{NAD}^+$  kinases known to date, NADKc displays unique structural  
17 as well as catalytic features which make it particularly suitable for rapid  $\text{NADP}^+$  production following  
18  $\text{Ca}^{2+}$  signals.

### 19 **Identification of a CaM-binding peptide in the NADKc N-terminal domain**

20 To verify that the NADKc N-terminal domain is involved in CaM-binding, we measured NADKc  
21 activity in the presence of a synthetic peptide containing the putative “type A 1-8-14” CaM-binding  
22 sequence (amino acids 167-196, Fig. 1C, Rhoads and Friedberg, 1997) in a competitive assay. As shown  
23 in Fig. 1E, the presence of the putative NADKc CaM-binding peptide decreased the stimulation of  
24 NADKc by AtCaM1, as expected if AtCaM1, trapped by the peptide in excess, was no longer available  
25 for NADKc activation. The reduction in reaction rate was hyperbolically related to the peptide  
26 concentration ( $\text{IC}_{50} = 0.5 \mu\text{M}$ ). In contrast, another unrelated peptide from the Tic32 protein, which

1 cannot specifically bind AtCaM1 (Dell'Aglio, 2013b), was also tested. An excess of this control peptide  
2 had no effect on NAD<sup>+</sup> kinase activity (Fig. 1E).

3 These data suggest that the NADKc peptide identified plays a major role in the AtCaM1/Ca<sup>2+</sup>-dependent  
4 activation of the NADKc enzyme. We hypothesize that it could be an anchoring point for CaM in the  
5 full-length protein, facilitating activation of the kinase domain by an as yet unknown mechanism.

## 6 **NADKc is located at the mitochondrial periphery**

7 To assess the NADKc localization *in vivo*, we produced strains containing several YFP-tagged NADKc  
8 versions: *i.*) the NADKc full-length protein fused to YFP at its C-terminal (construct NADKc-YFP); *ii.*)  
9 the NADKc N-terminal region (amino acids 1-45) fused to YFP (construct NADK<sub>C<sub>Nter</sub></sub>-YFP); the YFP  
10 fused at the N-terminus of the whole NADKc protein sequence (construct YFP-NADKc). All fusion  
11 proteins were inserted into expression plasmids under the control of the CaMV 35S promoter.

12 Arabidopsis lines and tobacco leaves containing the NADKc:YFP construct showed protein clusters that  
13 likely constitute non-specific aggregates caused by high expression of a membrane construct (not  
14 shown). However, in tobacco leaves (see Fig. S4, upper and middle row) and Arabidopsis seedlings, the  
15 NADK<sub>C<sub>Nter</sub></sub>-YFP was targeted to ring-like structures in both stomata (Fig. 2 A-F) and root tip cells. In  
16 the root tips, the NADK<sub>C<sub>Nter</sub></sub>-YFP protein co-localized with the mitochondrial matrix marker  
17 Tetramethylrhodamine, methyl ester (TMRM), but the fluorescence signal of NADK<sub>C<sub>Nter</sub></sub>-YFP was more  
18 peripheral than the TMRM signal (Fig. 2, G-I). As a comparison, we observed Arabidopsis root tip cells  
19 expressing NMT1-GFP, an outer mitochondrial membrane protein (Fig. 2, J-L, Wagner et al., 2015), as  
20 well as MT-cp-YFP (Fig. 2, M-O), a pH biosensor located in the mitochondrial matrix (Schwarzländer  
21 et al., 2011; Behera et al., 2018). This comparison clearly showed a higher resemblance of the  
22 NADK<sub>C<sub>Nter</sub></sub>-YFP signal profile to the NMT1-GFP profile than to the MTcp-YFP profile, suggesting a  
23 localization at the outer mitochondrial membrane.

24 To corroborate this conclusion we measured the pixel intensity distribution of various TMRM-stained  
25 mitochondria from NADK<sub>C<sub>Nter</sub></sub>-YFP transformed plants. While the TMRM fluorescence intensity peak  
26 was located at the centre of the mitochondria, NADK<sub>C<sub>Nter</sub></sub>-YFP fluorescence intensity formed two



1 distinctive peaks at opposite sides from the centre where fluorescence intensity was at its minimum (Fig.  
2 2, P-R). This pattern matches the one previously measured for the outer-membrane localized NMT1-  
3 GFP protein (Wagner et al, 2015).

4 We successfully achieved expression of YFP-NADKc only in transiently transformed tobacco leaves,  
5 where fluorescence was dispersed inside the cytosol (Fig. S4, bottom line). This result was probably due  
6 to the NADKc N-terminus being hidden in the middle of the sequence and is consistent with the  
7 hypothesis that the N-terminal region of NADKc is important for the protein to be correctly addressed  
8 to the mitochondria.

9 Protein overexpression by a strong promoter as CaMV 35S is prone to promote protein aggregates and  
10 overexpression artefacts. However, using cell fractionation, early works on the CaM/Ca<sup>2+</sup>-dependent  
11 NAD<sup>+</sup> kinase activity in plants located this enzyme at the mitochondrial periphery (either inner or outer  
12 mitochondrial membrane) in both maize (Dieter and Marmé, 1984; Sauer and Robinson, 1985) and  
13 *Avena sativa* (Pou de Crescenzo et al., 2001). More recently, NADKc was detected in the mitochondria  
14 by two proteomic studies (Klodmann et al., 2011, Wagner et al., 2015) and at the plasma membrane by  
15 one study (Mitra et al., 2009). Our results therefore corroborate and extend previous findings obtained  
16 using different approaches.

### 17 **NADKc enhances Flg22 response in Arabidopsis seedlings**

18 To investigate the physiological role of NADKc, we analysed the two Arabidopsis T-DNA insertion  
19 lines SALK\_006202 and GABI-KAT 311H11, hereafter called *nadkc-1* and *nadkc-2* (Fig. 3A). NADKc  
20 transcripts were reduced by more than 95% in both lines (Fig. 3B).

21 To confirm the unique role of NADKc for CaM/Ca<sup>2+</sup>-dependent NADP<sup>+</sup> production in Arabidopsis  
22 seedlings, NAD<sup>+</sup> kinase activity was measured in protein extracts from Col-0 and mutant seedlings, both  
23 in the presence of trifluoroperazine (TFP) - a CaM inhibitor - and AtCaM1/Ca<sup>2+</sup> (Fig. 3C). In Col-0  
24 plants, the activity measured in the presence of AtCaM1/Ca<sup>2+</sup> was more than 10-fold higher than in the  
25 presence of TFP, while in *nadkc-1/2* mutants, no difference was observed between the two conditions.  
26 In both mutants, activity levels were close to those measured in Col-0 plants in the presence of TFP,

1 confirming the absence of NADKc activity in these mutants. Consistent with these results, two  
2 complemented lines obtained by stably transforming *nadkc-1* with full-length NADKc under the control  
3 of the CaMV 35S promoter (lines *nadkc-1\_NADKc-1* and *nadkc-1\_NADKc-2*) - had NADKc activity  
4 levels similar to Col-0 (Fig. 4D).

5 Neither *nadkc* mutant showed any visible growth impairment when grown under short day or long day  
6 photoperiods (Fig. S5, A-B) and photosynthetic parameters (Fv/Fm, ETR and NPQ, (Maxwell and  
7 Johnson, 2000)) were the same in all genotypes (Fig. S5, C-E). This suggests that NADKc is not  
8 involved in photosynthesis-driven growth.

9 As CaM-dependent NAD<sup>+</sup> kinase activity was previously associated with the generation of the oxidative  
10 burst triggered by plant response to elicitors (Grant et al., 2000; Harding et al., 1997), we expected to  
11 observe a decrease in a pathogen elicitor-induced extracellular ROS burst in *nadkc-1/2* mutants coupled  
12 with lower NADP pools with respect to Col-0 seedlings.

13 We therefore exposed 7-day-old Arabidopsis seedlings to the bacterial elicitor flg22, followed by  
14 measurements of NAD(P)<sup>+</sup> and NAD(P)H concentrations and ROS production. As shown in Fig. 3E, no  
15 statistically significant differences were observed between Col-0 and *nadkc-1* in NAD(P)<sup>+</sup> and  
16 NAD(P)H concentrations before the flg22 treatment. However, the flg22 challenge induced an increase  
17 in the Col-0 NADP<sup>+</sup> cellular concentration, which was absent in the *nadkc* seedlings. Moreover,  
18 dramatic reduction in ROS accumulation (more than 90%) was observed in the *nadkc-1/2* mutants (Fig.  
19 3F), but complementation with the NADKc full-length protein restored ROS accumulation up to wild-  
20 type levels (Fig. 3G).

21 Based on these results, we propose a role for NADKc in producing NADP(H) needed to sustain the  
22 elicitor-induced ROS burst in Arabidopsis seedlings (Fig. 4).

### 23 **Distribution of CaM-dependent NAD<sup>+</sup> kinase activity in the green lineage**

24 The domain organization of NADKc (*i.e.*, a ca 200 amino acid domain of unknown function at the N-  
25 terminus with a putative CBS followed by a kinase domain annotated “zeta toxin domain”, Fig. 1C) was  
26 only found in higher plants and some algae.

1 To better trace the evolution of the plant CaM-dependent NAD<sup>+</sup> kinase, we compared gene sequences  
2 and NADK activity in several plants and algae and we built a maximum likelihood phylogenetic tree  
3 with representative putative NADKc proteins (Fig. S6). The phylogenetic tree showed that plant  
4 NADKc-like proteins form four major clusters that correspond to the main plant phylogenetic groups  
5 with the exception of Gymnosperms and Pteridophytes. Many plants, especially dicots, contain several  
6 genes encoding for this protein, suggesting duplication events across evolution. Interestingly, the two  
7 other NADKc homologues present in the Arabidopsis genome (At1g06750 and At2g30630) seem to  
8 have a pollen-specific expression pattern (Krishnakumar et al., 2014).

9 Among algae, while the genomes of *Chlamydomonas reinhardtii*, *Ostreococcus taurii* and *Chara*  
10 *braunii* appeared devoid of NADKc-like sequences, the genomes of *Coccomyxa subellipsoidea*, *Ulva*  
11 *mutabilis*, *Klebsormidium flaccidum*, *Spyrotaenia minuta*, *Entransia fimbriata*, Mougeotia sp. and  
12 Spirogyra sp. all harbour one NADKc-like sequence. In particular, NAD<sup>+</sup> kinase genes of  
13 *Klebsormidium flaccidum*, *Entransia fimbriata*, Mougeotia sp. and Spirogyra sp. contain a clear CBS,  
14 while in *Coccomyxa subellipsoidea*, *Ulva mutabilis* and *Spirotaenia minuta*, this region is less conserved  
15 (Fig. S2A). In agreement with the genomic survey, CaM-dependent NAD<sup>+</sup> kinase activity could be  
16 successfully measured in the moss *M. polymorpha* and filamentous alga *K. flaccidum*, but not in the  
17 unicellular alga *C. reinhardtii* (Table 2).

18 Interestingly, both the total CaM-dependent NAD<sup>+</sup> kinase activity and the percentage of CaM-dependent  
19 NADK-activity on the total NADK activity increase from *K. flaccidum* (4.0 nmol·h<sup>-1</sup>·mg<sup>-1</sup>; 66.7%) to  
20 *M. polymorpha* (5.9 nmol·h<sup>-1</sup>·mg<sup>-1</sup>; 85.7%) and to *A. thaliana* (30.2 nmol·h<sup>-1</sup>·mg<sup>-1</sup>; 96.8%). It is  
21 therefore possible that the importance of the CaM control on NADKc-like proteins increased during the  
22 evolution of plant lineage and became a key element of the ROS response to elicitors in angiosperms,  
23 and quite likely other abiotic/biotic stress conditions that trigger Ca<sup>2+</sup> fluxes.

## 24 **Conclusions**

25 Overall, we have identified unambiguously NADKc as the CaM/Ca<sup>2+</sup>-dependent NAD<sup>+</sup> kinase of  
26 Arabidopsis seedlings. Its identification allows answering earlier questions concerning its physiological

1 role: consistent with its localization at the mitochondrial periphery, this enzyme has no role in  
2 photosynthesis, but can regulate the ROS burst by sustaining the activity of RBOH proteins. Besides  
3 being essential for the elicitor-induced oxidative burst of Arabidopsis, this enzyme may participate in  
4 other plant developmental and stress responses involving  $\text{Ca}^{2+}$  fluxes. This would stem from the  
5 evolutionary recruitment of a distinctive combination of a CaM-binding region and a type II zeta-toxin  
6 domain, which would provide it with regulatory properties different from its animal counterpart.

7

## 8 **Material and Methods**

### 9 **Chemicals**

10 All chemicals were from Sigma Aldrich.

### 11 **Plant growth and isolation of homozygous NADKc lines**

12 *A. thaliana* Col-0 ecotype was used in this study. Plants were grown under 65% humidity and either  
13 long day (16 h light – 85  $\mu\text{mol photons}\cdot\text{m}^{-2}\cdot\text{s}^{-1}$ , 8 h dark) or short day (8 h light – 90  $\mu\text{mol photons}\cdot\text{m}^{-2}\cdot\text{s}^{-1}$ , 16 h dark) conditions. Day-time temperature was set to 20 °C, and night-time temperature to 18  
14 °C.  
15 °C.

16 The two T-DNA insertion lines, *nadkc-1* (SALK\_006202) and *nadkc-2* (GABI\_311H11), were obtained  
17 from NASC/ABRC (Alonso et al., 2003; Kleinboelting et al., 2012). Lines were selected in the  
18 appropriate antibiotic (kanamycin for *nadkc-1* and sulfadiazine for *nadkc-2*) and genotyped by PCR  
19 using left border primers LBb1.3 (*nadkc-1*) or LB GABI-KAT (*nadkc-2*) and the appropriate specific  
20 primers listed in Supplemental Table S2. PCR products were sequenced to confirm the precise position  
21 of each insertion.

22 *Klebsormidium flaccidum* (Hori et al., 2014) (SAG335-2b curated as *Klebsormidium nitens*) was  
23 obtained from EPSAG (Department of Experimental Phycology and Culture Collection of Algae,  
24 Göttingen Universität, Germany). The alga was grown on agar plates under continuous light (60  $\mu\text{mol}$

1 photons·m<sup>-2</sup>·s<sup>-1</sup>) in the Modified Bolds 3N Medium (<https://utex.org/products/modified-bolds-3n>  
2 medium) without vitamins.

3 *M. polymorpha* was collected in the forest (GPS coordinate: 45.335088 , 5.632257) and *Chlamydomonas*  
4 *reinhardtii* (C137 strain) was grown in TAP medium at 24°C under continuous low white light (40 μmol  
5 photons·m<sup>-2</sup>·s<sup>-1</sup>) exposure. Protein extracts were prepared as described in the supplementary information  
6 for Arabidopsis.

7 Additional Material and Methods procedures are described in the Supplementary Information.

### 8 **Author contributions**

9 E.D., C.M., G.F. and G.C. designed the experiments and analyzed the data; E.D., C.G., M.M., A.K.,  
10 Y.C., A.C. G.F., C.M., G.D., Y.G. and G.C. conducted the experiments. E.D., G.F., C.M. and G.C. wrote  
11 the article with contributions from all the authors. G.C. agrees to serve as the author responsible for  
12 contact and ensures communication.

### 13 **Accession numbers**

14 Sequence data from this article can be found in the EMBL/GenBank data libraries under accession  
15 number: At1g04280; UniProt accession: Q0WUY1.

16

### 17 **Acknowledgments**

18 This work was supported by the French National Research Agency (grant no. ANR-10-13 LABEX-04  
19 GRAL Labex, Grenoble Alliance for Integrated Structural Cell Biology). G.F. acknowledges support  
20 from the HFSP grant RGP0052/2015 (photosynthetic light utilization and ion fluxes: making the link)  
21 and A.C. to UNIMI PIANO DI SVILUPPO DI ATENEO, Transition Grant 2015/2017 – Horizon 2020  
22 Linea 1A. The proteomic analyses were partially supported by the French National Research Agency  
23 ProFI Grant (ANR-16 10-INBS-08-01). Part of this work was carried out at NOLIMITS, an advanced  
24 imaging facility established by the University of Milan.

1 We are grateful to Markus Schwarzländer (University of Münster, Germany) for providing the  
2 NMT1:GFP and MT-cp:YFP Arabidopsis lines. We thank Elsa Clavel-Coibrié for help with analysis of  
3 the complemented mutant plants.

#### 4 **References**

- 5 **Alonso JM, Stepanova AN, Leisse TJ, Kim CJ, Chen H, Shinn P, Stevenson DK,**  
6 **Zimmerman J, Barajas P, Cheuk R, et al** (2003) Genome-wide insertional mutagenesis of  
7 *Arabidopsis thaliana*. *Science* **301**: 653-657
- 8 **Anderson JM, Cormier MJ** (1978) Calcium-dependent regulation of NAD kinase. *Biochem*  
9 *Biophys Res Commun* **84**: 595-602
- 10 **Behera S, Zhaolong X, Luoni L, Bonza MC, Doccua FG, De Michelis MI, Morris RJ,**  
11 **Schwarzländer M, Costa A** (2018) Cellular Ca<sup>2+</sup> signals generate defined pH signatures in plants. *Plant*  
12 *Cell* **30**: 2704-2719
- 13 **Chai MF, Wei PC, Chen QJ, An R, Chen J, Yang S, Wang XC** (2006) NADK3, a novel  
14 cytoplasmic source of NADPH, is required under conditions of oxidative stress and modulates abscisic  
15 acid responses in Arabidopsis. *Plant J* **47**: 665-674
- 16 **Chapman JM, Muhlemann JK, Gayomba SR, Muday GK** (2019) RBOH-Dependent ROS  
17 Synthesis and ROS scavenging by plant specialized metabolites to modulate plant development and  
18 stress responses. *Chem Res Toxicol.* **32**: 370-396
- 19 **Choi WG, Miller G, Wallace I, Harper J, Mittler R, Gilroy S** (2017) Orchestrating rapid long-  
20 distance signaling in plants with Ca<sup>2+</sup>, ROS and electrical signals. *Plant J* **90**: 698-707
- 21 **Dell'Aglio E, Giustini C, Salvi D, Brugiere S, Delpierre F, Moyet L, Baudet M, Seigneurin-**  
22 **Berny D, Matringe M, Ferro M, et al** (2013a) Complementary biochemical approaches applied to the  
23 identification of plastidial calmodulin-binding proteins. *Mol Biosyst* **9**: 1234-1248
- 24 **Dell'Aglio E** (2013b) The regulation of plastidial proteins by calmodulins: Université de  
25 Grenoble.
- 26 **Delumeau O, Renard M, Montrichard F** (2000b) Characterization and possible redox  
27 regulation of the purified calmodulin-dependent NAD<sup>+</sup> kinase from *Lycopersicon pimpinellifolium*.  
28 *Plant Cell Environ* **23**: 1267-1273
- 29 **Dieter P, Marme D** (1984) A Ca<sup>2+</sup>, Calmodulin-dependent NAD kinase from corn is located in  
30 the outer mitochondrial membrane. *J Biol Chem* **259**: 184-189
- 31 **Drerup MM, Schlücking K, Hashimoto K, Manishankar P, Steinhorst L, Kuchitsu K, Kudla**  
32 **J.** (2013) The Calcineurin B-like calcium sensors CBL1 and CBL9 together with their interacting protein  
33 kinase CIPK26 regulate the Arabidopsis NADPH oxidase RBOHF. *Mol Plant.* **6**: 559-69
- 34 **Dubiella U, Seybold H, Durian G, Komander E, Lassig R, Witte CP, Schulze WX, Romeis**  
35 **T** (2013) Calcium-dependent protein kinase/NADPH oxidase activation circuit is required for rapid  
36 defense signal propagation. *Proc Natl Acad Sci USA.* **110**: 8744-9
- 37 **Grant M, Brown I, Adams S, Knight M, Ainsli A, Mansfield J** (2000) The RPM1 plant disease  
38 resistance gene facilitates a rapid and sustained increase in cytosolic calcium that is necessary for the  
39 oxidative burst and hypersensitive cell death. *Plant J* **23**: 441-450

- 1           **Harding SA, Oh SH, Roberts DM** (1997) Transgenic tobacco expressing a foreign calmodulin  
2 gene shows an enhanced production of active oxygen species. *Embo J* **16**: 1137-1144
- 3           **Kawai S, Mori S, Mukai T, Hashimoto W, Murata K** (2001) Molecular characterization of  
4 *Escherichia coli* NAD kinase. *Eur J Biochem* **268**: 4359-65
- 5           **Khoo SK, Loll B, Chan WT, Shoeman RL, Ngoo L, Yeo CC, Meinhart A** (2007) Molecular  
6 and structural characterization of the PezAT chromosomal toxin-antitoxin system of the human  
7 pathogen *Streptococcus pneumoniae*. *J Biol Chem* **282**: 19606-19618
- 8           **Kleinboelting N, Huet G, Kloetgen A, Viehoveer P, Weisshaar B** (2012) GABI-Kat  
9 SimpleSearch: new features of the *Arabidopsis thaliana* T-DNA mutant database. *Nucleic Acids Res*  
10 **40**: D1211-1215
- 11           **Klodmann J, Senkler M, Rode C, Braun H-P** (2011) Defining the protein complex proteome  
12 of plant mitochondria. *Plant Phys* **157**: 587–598
- 13           **Krishnakumar V, Hanlon MR, Contrino S, Ferlanti ES, Karamycheva S, Kim M, Rosen**  
14 **BD, Cheng C-Y, Moreira W, Mock SA, Stubbs J, Sullivan JM, Krampis K, Miller JR, Micklem**  
15 **G, Vaughn M, Town CD** (2015) Araport: the Arabidopsis information portal. *Nucleic Acids Research*  
16 **43**: D1003–D1009
- 17           **Love NR, Pollak N, Dolle C, Niere M, Chen Y, Oliveri P, Amaya E, Patel S, Ziegler M** (2015)  
18 NAD kinase controls animal NADP biosynthesis and is modulated via evolutionarily divergent  
19 calmodulin-dependent mechanisms. *Proc Natl Acad Sci USA* **112**: 1386-1391
- 20           **Liebthal M, Dietz KJ** (2017) The fundamental role of reactive oxygen species in plant stress  
21 response. *Plant Stress Tolerance In: Sunkar R. (eds) Plant Stress Tolerance. Methods in Molecular*  
22 *Biology*, **1631**: 23-39. Humana Press, New York, NY.
- 23           **Maxwell K, Johnson GN** (2000) Chlorophyll fluorescence-a practical guide. *J Exp Bot* **51**: 659-  
24 668.
- 25           **Mhamdi A, Mauve C, Gouia H, Saindrenan P, Hodges M, Noctor G** (2010) Cytosolic NADP-  
26 dependent isocitrate dehydrogenase contributes to redox homeostasis and the regulation of pathogen  
27 responses in Arabidopsis leaves. *Plant Cell Env* **33**: 1112-1123
- 28           **Mitra SK, Gantt JA, Ruby JF, Clouse SD, Goshe MB** (2007) Membrane proteomic analysis  
29 of *Arabidopsis thaliana* using alternative solubilization techniques. *J. Proteome Res.* **6**: 1933-1950
- 30           **Pou de Crescenzo M-A, Gallais S, Léon A, Laval-Martin DL** (2001) Tween-20 activates and  
31 solubilizes the mitochondrial membrane-bound, calmodulin dependent NAD<sup>+</sup> kinase of *Avena sativa* L.  
32 *J Membr Biol* **182**: 135–146
- 33           **Pugin A, Frachisse JM, Tavernier E, Bligny R, Gout E, Douce R, Guern J** (1997) Early events  
34 induced by the elicitor cryptogein in tobacco cells: involvement of a plasma membrane NADPH oxidase  
35 and activation of glycolysis and the pentose phosphate pathway. *Plant Cell* **9**: 2077-2091
- 36           **Rhoads AR, Friedberg F** (1997) Sequence motifs for calmodulin recognition. *The FASEB*  
37 *Journal* **11**: 331–340
- 38           **Sauer A, Robinson DG** (1985) Calmodulin dependent NAD-kinase is associated with both the  
39 outer and inner mitochondrial membranes in maize roots. *Planta* **166**: 227-233
- 40           **Scharte J, Schön H, Tjaden Z, Weis E, von Schaewen A** (2009) Isoenzyme replacement of  
41 glucose-6-phosphate dehydrogenase in the cytosol improves stress tolerance in plants. *Proc Natl Acad*  
42 *Sci U S A* **106**: 8061-8066

1           **Schwarzländer M, Logan DC, Fricker MD, Sweetlove LJ** (2011) The circularly permuted  
2 yellow fluorescent protein cpYFP that has been used as a superoxide probe is highly responsive to pH  
3 but not superoxide in mitochondria: implications for the existence of superoxide 'flashes'. *Biochem J.*  
4 **437**: 381-7

5           **Torres MA, Dangl JL** (2005) Functions of the respiratory burst oxidase in biotic interactions,  
6 abiotic stress and development. *Curr Opin Plant Biol* **8**: 397-403

7           **Turner WL, Waller JC, Vanderbeld B, Snedden WA** (2004). Cloning and characterization of  
8 two NAD kinases from Arabidopsis. Identification of a calmodulin binding isoform. *Plant Physiol* **135**:  
9 1243-1255

10           **Wagner S, Behera S, De Bortoli S, Logan DC, Fuchs P, Carraretto L, Teardo E, Cendron**  
11 **L, Nietzel T, Füßl M, Doccua FG, Navazio L, Fricker MD, Van Aken O, Finkemeier I, Meyer AJ,**  
12 **Szabò I, Costa A, Schwarzländer M** (2015) The EF-hand Ca<sup>2+</sup> binding protein MICU choreographs  
13 mitochondrial Ca<sup>2+</sup> dynamics in Arabidopsis. *The Plant Cell* **27**: 3190–3212

14

## 15 **Figures legends**

16 **Figure 1.** Biochemical properties of a CaM-dependent NAD<sup>+</sup> kinase identified in Arabidopsis. (A)  
17 NAD<sup>+</sup> kinase activity measured in an *E. coli* extract expressing an empty pET28b(+) and an *E. coli*  
18 extract expressing At1g04280. Spikes correspond to the moments of addition of glucose 6-phosphate  
19 dehydrogenase (G6PDH), Ca<sup>2+</sup>, AtCaM1, and *E. coli* extracts (10 µg). (B) NAD<sup>+</sup> kinase activity in an  
20 *E. coli* bacterial extract expressing At1g04280. Ca<sup>2+</sup>, AtCaM1 and EGTA were added at different times,  
21 as indicated in the graph. (C) Schematic representation of the NADKc primary sequence and comparison  
22 with previously known NAD<sup>+</sup> kinases. Yellow: zeta-toxin domain (InterPro Homologous superfamily:  
23 IPR010488); black: N-terminal region with putative organelle target sequence; red: putative conserved  
24 Type A 1-8-14 CaM-binding site (detailed below the scheme); orange: Walker A motif (ATP-binding  
25 site); blue: NAD<sup>+</sup> kinase domain (InterPro Homologous Superfamily: IPR016064); red/grey: N-terminal  
26 sequence expected to contain a CaM-binding site according to Love et al, 2015. Sequences used for  
27 comparison (UniProt): *E. coli* NAD<sup>+</sup> kinase: P0A7B3; *A. thaliana* NAD<sup>+</sup> kinases: AtNADK1: Q56YN3;  
28 AtNADK2: Q9C5W3; AtNADK3: Q500Y9; *Strongylocentrotus purpuratus* NAD<sup>+</sup> kinase-2 (sea urchin  
29 CaM-dependent NAD<sup>+</sup> kinase, Love et al., 2015): C3RSF7. (D) Affinity of NADKc recombinant protein  
30 for AtCaM1: Activity of the purified NADKc recombinant protein after denaturation in urea and  
31 subsequent refolding was measured in the presence of 50 µM Ca<sup>2+</sup> and as a function of [AtCaM1].  
32 Experiments were performed in triplicate and data shown are from one representative experiment.



1 Binding data were analysed assuming tight binding.  $K_d$  value for AtCaM1 binding varied from 0.6 to 1  
2 nM. (E) Inhibition of NADKc activity by competition with the putative CaM-binding site (black dots).  
3 Black squares correspond to results obtained with a negative control peptide, which does not bind  
4 AtCaM1.

5 **Figure 2.** Analysis of submitochondrial localization of NADK<sub>C<sub>Nter</sub></sub>-YFP. (A to C) Confocal laser  
6 scanning microscopy images from stomata guard cells of a representative Arabidopsis seedling stably  
7 expressing NADK<sub>C<sub>Nter</sub></sub>-YFP. Scale bar = 5  $\mu$ m. (D to E) Higher magnification of the region of interest  
8 shown in A to C (white squares). Scale bar = 1  $\mu$ m. (A, D) YFP fluorescence in green; (B, E) chlorophyll  
9 fluorescence in blue; (C, F) merge between YFP and chlorophyll fluorescences. (G to I) Confocal laser  
10 scanning microscopy images from root tip cells of a representative Arabidopsis seedling stably  
11 expressing NADK<sub>C<sub>Nter</sub></sub>-YFP and stained with the mitochondrial matrix marker TMRM. Scale bar = 1  
12  $\mu$ m. (J to L) Confocal laser scanning microscopy images from root tip cells of a representative  
13 Arabidopsis seedling stably expressing NMT-GFP and stained with the mitochondrial matrix marker  
14 TMRM. Scale bar = 1  $\mu$ m. (M to O) Confocal laser scanning microscopy images from root tip cells of  
15 a representative Arabidopsis seedling stably expressing MT-cpYFP and stained with the mitochondrial  
16 matrix marker TMRM. Scale bar = 1  $\mu$ m. (G, M) YFP fluorescence in green; (J) GFP fluorescence in  
17 green; (H, K and N) TMRM fluorescence in magenta; (I, L and O) merge between YFP/GFP and TMRM  
18 fluorescences. NMT1-GFP and MT-cpYFP were used as markers for the mitochondrial outer  
19 mitochondrial membrane (OMM) and matrix, respectively. (P to R) Normalized pixel intensity  
20 distributions in the YFP and TMRM fluorescence channels plotted centrally across three individual  
21 mitochondria of a seedling expressing the NADK<sub>C<sub>Nter</sub></sub>-YFP.

22 **Figure 3.** The CaM/Ca<sup>2+</sup>-dependent NAD<sup>+</sup> kinase activity of Arabidopsis seedlings is absent in *nadkc*  
23 mutants. (A) schematic representation of the NADKc gene and position of the T-DNA insertions in the  
24 *nadkc-1* and *nadkc-2* mutant lines. (B) NADKc transcript levels in Col-0 and *nadkc*-mutant seedlings.  
25 Levels are expressed relative to GAPDH. Data shown correspond to mean +/- s.d., n=3. (C) NAD<sup>+</sup>  
26 kinase activity measured in Col-0 and *nadkc* mutant plants (7-day-old whole plantlets), in the presence  
27 of the CaM inhibitor TFP (40  $\mu$ M) or AtCaM1 (250 nM) and Ca<sup>2+</sup> (0.5 mM). Values correspond to the  
28 average of four replicates. (D) NAD<sup>+</sup> kinase activity measured in Col-0 and mutant plants complemented

1 with NADKc gene (*nadkc-1\_NADKc-1* and *nadkc-1\_NADKc-2*) in 7-day-old whole plantlets, in the  
2 presence of the CaM inhibitor TFP (40  $\mu$ M) or of AtCaM1 (250 nM) and Ca<sup>2+</sup> (0.5 mM). (E) NAD(P)<sup>+</sup>  
3 and NAD(P)H concentrations in 7-day-old seedlings exposed (flg22, 1  $\mu$ M) or unexposed (H<sub>2</sub>O) for 12  
4 min. to the bacterial elicitor flagellin22. (80-100 mg of tissue per measure, data shown correspond to  
5 mean +/- s.e.m. for 3 biological replicates). (F) Flg22 (1  $\mu$ M)-induced oxidative burst in 7-day-old Col-  
6 0 and *nadkc* mutant seedlings (30 plantlets per well, data shown correspond to mean +/- s.d. for 4 wells).  
7 (G) Flg22 (1  $\mu$ M)-induced oxidative burst in Col-0, *nadkc-1* mutant and mutant plants complemented  
8 with NADKc gene (*nadkc-1\_NADKc-1* and *nadkc-1\_NADKc-2*); 7-day-old seedlings, 30 plantlets per  
9 well. Data shown correspond to mean +/- s.d. for 4 wells. Asterisks indicate a significant difference  
10 between two conditions based on a Welch's t test (\*p < 0.05; \*\*\*p < 0.001).

11 **Figure 4.** Hypothetical model of the role of CaM/Ca<sup>2+</sup>-dependent NADKc in sustaining the flg22-  
12 induced oxidative burst in Arabidopsis seedlings. Numbers refer to known sequential events; red  
13 numbers highlight events related to NADKc activation: 1. binding of Flg22 elicitor to the Fls2 receptor  
14 (Sun et al., 2013); 2. activation of proton efflux and Ca<sup>2+</sup> influx; 3a. Ca<sup>2+</sup>-dependent activation of CDPKs  
15 and CIPK/CBLs that phosphorylate RBOH proteins; 3b. Ca<sup>2+</sup> binding to RBOH proteins; 3c. Ca<sup>2+</sup>  
16 binding to CaM, leading to CaM structural modification and formation of the CaM/NADKc complex;  
17 4. activation of NADP<sup>+</sup> production by NADKc; 5. increased flux in the oxidative pentose phosphate  
18 pathway (OPPP), leading to a higher availability of NADPH; 6. production of the extracellular oxidative  
19 burst by NADPH oxidases (RBOH proteins).

20 **Table 1.** NADKc kinetic parameters.

21 **Table 2.** Comparison of CaM-dependent NADK activity in different photosynthetic organisms. NADK  
22 activity (nmol·h<sup>-1</sup>·mg<sup>-1</sup> protein) was measured in soluble protein extracts from *Arabidopsis thaliana*,  
23 *Marchantia polymorpha*, *Klebsormidium flaccidum* and *Chlamydomonas reinhardtii* as detailed in  
24 Methods. Activities are expressed in nmol/h/mg protein. <sup>a</sup>NADK activity measured in the presence of  
25 CaM/Ca<sup>2+</sup> represents CaM-independent plus CaM-dependent activity; <sup>b</sup>NADK activity measured in the  
26 presence of trifluoroperazine (CaM inhibitor) represents CaM-independent NADK activity. <sup>c</sup>CaM/Ca<sup>2+</sup>-  
27 dependent activity is the difference between total NADK activity and CaM/Ca<sup>2+</sup>-independent activity.

1 NADK activity in *C. reinhardtii* is independent on CaM/Ca<sup>2+</sup> (the difference is within experimental  
2 error).

### 3 **Supplemental Material and Methods**

#### 4 **Partial purification of native NADKc**

5 To purify native CaM-dependent NAD<sup>+</sup> kinase, Col-0 Arabidopsis plants seeds were sterilized, sown in  
6 Murashige and Skoog (Murashige and Skoog, 1962) liquid medium (2.2 g L<sup>-1</sup>) supplemented with 0.5 g  
7 L<sup>-1</sup> sucrose and grown under continuous light (60 μE) in 250-mL flasks and under agitation (125 rpm).  
8 Seven-day-old plants were rinsed with water, frozen in liquid nitrogen and ground with a mortar and  
9 pestle. The powder was suspended in Buffer A (50 mM Tris-HCl pH 7.5, 400 mM KCl, 3 mM MgCl<sub>2</sub>,  
10 1 mM EGTA, 0.5 mM EDTA, 1 mM DTT, 1 mM NAD<sup>+</sup>, 10 μM leupeptine, 10 μM E64, 1 mM PMSF,  
11 1 mM benzamidine and 5 mM ε-aminocaproic acid). The crude extract was centrifuged (15,000 g, 30  
12 min, 4 °C) and the recovered soluble protein extract (432 mg, 72 mL, 0.74 μmol h<sup>-1</sup> mg<sup>-1</sup>) was  
13 precipitated with 50% ammonium sulfate (1 h, 4 °C) and centrifuged (20,000 g, 20 min). The protein  
14 pellet was then suspended in 32 mL Buffer A (30 mL, 270 mg, 1.1 μmol h<sup>-1</sup> mg<sup>-1</sup>) and loaded onto a  
15 DEAE column (60 mL resin) equilibrated with Buffer A. AtCaM1/Ca<sup>2+</sup>-dependent NADK activity was  
16 detected in the flow-through (120 mL, 84 mg, 1.8 μmol h<sup>-1</sup> mg<sup>-1</sup>). NaCl (3.5 M) was added to this  
17 fraction, and the protein solution was loaded onto a Butyl-Sepharose column (12 mL resin) equilibrated  
18 with Buffer B - NaCl (50 mM Tris-HCl pH 7.0, 3.5 M NaCl, 100 mM KCl, 3 mM MgCl<sub>2</sub>, 1 mM DTT).  
19 Elution was performed by applying a linear gradient (60 mL) from 0 to 100% Buffer B-ethane diol (50  
20 mM Tris-HCl pH 7.5, 30% ethane diol (v/v), 100 mM KCl, 3 mM MgCl<sub>2</sub>, 1 mM DTT). Eluted fractions  
21 containing AtCaM1/Ca<sup>2+</sup>-dependent NADK activity were supplemented with 1 mM NAD<sup>+</sup> and  
22 immediately frozen. Fractions were pooled (5.6 mg, 2.32 μmol h<sup>-1</sup> mg<sup>-1</sup>, 8 mL) before loading onto a 1-  
23 mL CaM-Sepharose column (Stratagen) equilibrated with buffer C (50 mM Tris pH 7.5, 10% (v/v)  
24 glycerol, 1 mM DTT, 2 mM CaCl<sub>2</sub>). The column was washed with 10 volumes Buffer C supplemented  
25 with 500 mM NaCl. Bound proteins were then eluted with 50 mM Tris pH 7.5, 10% (v/v) glycerol, 1  
26 mM DTT and 5 mM EGTA. The fraction with highest activity (3 μg, 100 μl, 577 μmol h<sup>-1</sup> mg<sup>-1</sup>) was  
27 used for LC-MS/MS analyses (Fig. S1).

## 1 **Mass spectrometry-based proteomic analyses**

2 Proteins from the eluate and flow-through fractions were stacked by performing a very short run on an  
3 SDS-PAGE gel (NuPAGE 4-12%, ThermoFisher Scientific). Proteins were revealed by staining with  
4 Coomassie blue (R250, Bio-Rad), and submitted to in-gel digestion using modified trypsin (Promega,  
5 sequencing grade), as previously described (Casabona et al., 2013).

6 Resulting peptides were analyzed by online nanoLC-MS/MS (UltiMate 3000 and LTQ23 Orbitrap Velos  
7 Pro, Thermo Scientific). Briefly, peptides were sampled on a 300  $\mu\text{m}$  x 5 mm PepMap C18 precolumn  
8 and separated on a 75  $\mu\text{m}$  x 250 mm C18 column (PepMap, Thermo Scientific). MS and MS/MS data  
9 were acquired using Xcalibur (Thermo Scientific). Peptides and proteins were identified using Mascot  
10 (version 2.6), performing concomitant searches against Uniprot (*A. thaliana* taxonomy), the classical  
11 contaminants database (in-house) and the corresponding reversed databases. Proline software  
12 (<http://proline.profiroteomics.fr>) was used to filter the results (conservation of rank 1 peptides, peptide  
13 identification FDR < 1% as calculated on peptide scores using the reverse database strategy, minimum  
14 peptide score of 25, and minimum of one specific peptide identified per protein group). Results from  
15 individual samples were compiled, and grouped before comparing protein groups from different  
16 samples. Proteins were considered to be enriched in the eluate if they were identified only in this sample  
17 with a minimum of five specific spectral counts, or if they were enriched at least 10-fold in this sample  
18 compared to flow-through sample. Relative quantification was performed on the basis of specific  
19 spectral counts.

## 20 **Recombinant protein expression and purification**

21 Full-length At1g04280 cDNA was amplified by PCR from a pYES cDNA library (Elledge et al., 1991)  
22 using the primers listed in Supplemental Table S2. The PCR products digested by Nde I and Xho I were  
23 ligated into a pet28b(+) vector digested by the same enzymes to produce the constructs named pet28(b)-  
24 6HIS-NADKc and pet28(b)-6HIS- $\Delta$ 38NADKc. The proteins were produced from these constructs with  
25 a 22-amino-acid N-terminal His-tag.

1 Rosetta2-competent cells were transformed by one or the other of these two constructs and grown at 37  
2 °C in the presence of Chloramphenicol (34 µg.mL<sup>-1</sup>) and Kanamycin (50 µg.mL<sup>-1</sup>) until Abs at 600 nm  
3 reached 0.6. IPTG (0.4 mM) was added, and growth was continued at 20 °C for 15 h. Bacteria were  
4 pelleted, suspended in Buffer D (50 mM HEPES pH 7.8, 500 mM KCl, 10% (v/v) glycerol, 50 mM L-  
5 arginine, 50 mM L-glutamate, 1 mM NAD<sup>+</sup>) supplemented with 1 mM benzamidine and 5 mM ε-  
6 aminocaproic acid, 1 mM β-mercaptoethanol, and lysed by sonication. Insoluble material was removed  
7 by centrifugation (15,000 g, 20 min, 4 °C), and soluble proteins were recovered. A much higher  
8 production level and higher activity were obtained with the 6HIS-Δ38-NADKc construct, therefore  
9 further work was performed with this protein. The protein extract (30 mL, 11.3 mg mL<sup>-1</sup>) was loaded  
10 onto a Ni-NTA Sepharose column (3 mL resin). After washing with buffer D supplemented with 50 mM  
11 imidazole (15 mL), the recombinant protein was eluted in buffer A supplemented with 250 mM  
12 imidazole. The imidazole concentration was reduced to 5 mM by protein-concentration cycles followed  
13 by dilution in buffer A. Pooled fractions containing NADKc activity were concentrated on 10K  
14 Vivascience concentrators, aliquoted, frozen in liquid N<sub>2</sub> and stored at -80 °C. After this first purification  
15 step, the protein fraction still contained small amounts of contaminating proteins. To improve  
16 purification, Ni-NTA-Sepharose fractions (2 mg, 2.2 mL) were denatured in 8 M urea and purified on  
17 Ni-NTA Sepharose under denaturing conditions (6 M urea). After washing with 15 mL buffer E (25  
18 mM Tris-Cl pH 8.0, 500 mM NaCl, 5 mM β-mercaptoethanol, 6 M urea) supplemented with 50 mM  
19 imidazole, the pure denatured protein was eluted in buffer E supplemented with 250 mM imidazole. The  
20 denatured protein (0.3 mL, 0.3 mg, lane 4, Fig. S4) was then refolded by drop-by-drop dilution in 15  
21 mL buffer D supplemented with 1 mM DTT. The refolding reaction was performed with mixing and at  
22 room temperature. The highly purified protein (lane 5, Fig. S4) was then concentrated as described  
23 above, aliquoted, frozen in liquid nitrogen and stored at -80 °C.

24 *A. thaliana* Calmodulin 1 (AtCaM1, At5g37780) was purified as previously described (Dell'Aglio et al.,  
25 2013a).

26 Proteins were quantified by the Bradford method, using bovine γ-globulin as a standard or, for purified  
27 proteins, by measuring A<sub>205nm</sub> (Scopes, 1974). CaM-binding peptide

1 (QKVPKDKDFVMAATRQKRFERVTKDLKVKR) was synthesized by Smart Bioscience (France).

2 The control peptide sequence was VKDTELAKKVWDFSTKLTDS (Dell'Aglio, 2013<sup>b</sup>).

### 3 **Activity measurements**

4 NADK activity in extracts prepared from Col-0 *A. thaliana* plants, *K. flaccidum*, *M. polymorpha* and *C.*  
5 *reinhardtii* was measured at 25 °C as previously described (Turner et al., 2004) in the presence of a CaM  
6 inhibitor (trifluoroperazine, 50 μM) or in the presence of AtCaM1 (1 μM) and Ca<sup>2+</sup> (500 μM) .  
7 Recombinant NADKc activity was measured in thermostatic cuvettes (25 °C) with 20 nM enzyme in  
8 the presence of 50 mM HEPES-KOH pH 7.8, 5 mM glucose-6-phosphate, 10 mM MgCl<sub>2</sub> and variable  
9 concentrations of NAD<sup>+</sup> and ATP (or other nucleotide), 30 mU of glucose-6-phosphate dehydrogenase  
10 from baker's yeast and, where indicated in the figure legends, 50 μM Ca<sup>2+</sup> and/or AtCaM1. NADPH  
11 production was detected by monitoring absorbance at 340 nm ( $\epsilon_{340\text{ nm}} = 6250\text{ M}^{-1}\text{ s}^{-1}$ ). Kinetic data  
12 reported in Table 1 were calculated by fitting enzymatic data to the appropriate theoretical equations  
13 using the Kaleidagraph program (Synergy Software, Reading, PA, USA). Tight binding of AtCaM1  
14 onto NADKc was fitted using Eqn. 1:

$$15 \quad v/[E]_0 = k_{cat} \frac{([CaM] + k_d + [E]_0) - \sqrt{([CaM] + k_d + [E]_0)^2 - 4 * k_d * [E]_0}}{2[E]_0}$$

16 (Eqn.1)

17 where  $k_{cat}$  is the catalytic constant for NADKc,  $[CaM]$  is the total CaM concentration,  $k_d$  is the  
18 dissociation constant for the interaction between CaM and NADKc, and  $[E]_0$  is the total NADKc  
19 concentration.

### 20 **Subcellular localization by confocal microscopy**

21 The N-ter of the protein (amino acids: 1-60) or the entire protein sequence was amplified by PCR from  
22 pet28(b)-6HIS-NADKc using the primers listed in Supplemental Table S2. The amplified PCR products  
23 were cloned into the Gateway-adapted vector pDONR211 by BP recombination, to produce  
24 pDONR:NADKc<sub>Nter</sub>, pDONR:NADKc and pDONR:NADKc<sub>STOP</sub> constructs.

1 These vectors were then recombined with pB7YWG2,0 and pB7WGY2,0 vectors (Karimi et al., 2007),  
2 respectively, to generate pB7YWG2:NADK<sub>C<sub>Nter</sub></sub>-YFP, pB7YWG2:NADK<sub>C</sub>-YFP and pB7WGY2:YFP-  
3 NADK<sub>C</sub> through the LR recombination reaction. All vectors were transformed into *Agrobacterium*  
4 *tumefaciens* C58 and used for tobacco leaf infiltration.

5 Transient expression in *Nicotiana benthamiana* var. Xanthi was performed by infiltrating leaves with a  
6 suspension of *A. tumefaciens* harboring pB7YWG2:NADK<sub>C<sub>Nter</sub></sub>-YFP and RFP fused with the first 69  
7 amino acids of ATP synthase subunit 9a mitochondrial marker (pSu9-RFP) (Michaud et al., 2014) or  
8 pB7WGY2:YFP:NADK<sub>C</sub>, and the silencing suppressor P19 protein.

9 Transformed samples were observed by confocal microscopy on a LSM 800 confocal microscope  
10 equipped with a Plan-Apo 63X/1.4 oil DIC lens, two GaAsP detectors and one Airyscan detector. YFP  
11 and RFP fluorophores were excited at 488 and 558 nm, respectively, and emission signals were  
12 measured at 488-560 nm for YFP, and at 568-611 nm for RFP.

13 Stable expression in *Arabidopsis thaliana* seedlings was achieved by transforming the localization  
14 vectors into *A. tumefaciens* C58, which was used for floral dipping transformation. Complemented lines  
15 were screened based on their BASTA-resistance.

16 Confocal microscopy analyses of stable transgenic *Arabidopsis* seedlings root and shoot cells were  
17 performed using a Nikon Eclipse Ti2 inverted microscope, equipped with a Nikon A1+ laser scanning  
18 device (Nikon). Images were acquired by a CFI Apochromat TIRF 100XC, 1.49 N.A., oil immersion.  
19 EGFP or YFP were excited with the 488 nm laser and the emission was collected at 525-550 nm. For  
20 co-localization studies with Tetramethylrhodamine, Methyl Ester, Perchlorate (TMRM) seedlings were  
21 dipped in the following solution: 10 mM MES, 5 mM KCl, 10 mM CaCl<sub>2</sub>, pH 5.8 with TRIS-base  
22 supplemented with 500 nM TMRM. TMRM was excited with the 561 nm laser and the emission was  
23 collected at 570-620 nm. Chlorophyll was excited with the 488 nm laser and the emission was collected  
24 at 663-738 nm. Pinhole was set to 0.6 (Figure 2A to F) or 0.8 (Figure 2G-O) airy unit and the images  
25 were acquired using 2048 x 2048 pixels. Pixel intensities of the YFP and TMRM fluorescences were  
26 extracted using FIJI software (<https://fiji.sc/>).

## 1 **Measurement of photosynthetic parameters**

2 Maximum quantum yield of photosystem II ( $F_v/F_m$ ), relative electron transport rate (ETR) and non-  
3 photochemical quenching (NPQ) were determined using a chlorophyll fluorescence imaging system  
4 (SpeedzenIII, JbeamBio, France)  $F_v/F_m: (F_m - F_o)/F_m$ ;  $ETR = ((F_m' - F_s)/F_m')$ ;  $NPQ = (F_m - F_m')/F_m'$ ;  
5 where  $F_m$  = maximum fluorescence;  $F_o$  = minimum fluorescence;  $F_v$  = variable fluorescence ( $F_v = F_m -$   
6  $F_o$ ) in dark-adapted state (Maxwell and Johnson, 2000).  $F_m'$ , maximum fluorescence in the light;  $F_s$ ,  
7 steady-state chlorophyll fluorescence. Plants were dark adapted for at least 30 minutes prior to  
8 measurement.

## 9 **Mutant complementation**

10 To complement the SALK\_006202 NADKc mutant line, the entire NADKc protein sequence was  
11 amplified by PCR from pet28(b)-6HIS-NADKc using the primers listed in Supplemental Table S1. The  
12 amplified PCR product was cloned into the Gateway-adapted vector pDONR211 by BP recombination,  
13 thus generating pDONR:NADKcSTOP. This vector was then recombined with pB2GW7,0 (Karimi et  
14 al., 2007) to generate pB2GW7:NADKc by the LR recombination reaction. This vector was transformed  
15 into *A. tumefaciens* C58 and used for floral dipping transformation. Complemented lines were screened  
16 based on their BASTA-resistance and AtCaM1/Ca<sup>2+</sup>- dependent NAD<sup>+</sup> kinase activity.

17 Lines for which levels of AtCaM1/Ca<sup>2+</sup>-dependent NAD<sup>+</sup> kinase activity were similar to wild-type  
18 plants were further analyzed.

## 19 **NAD(P)<sup>+</sup> measurements**

20 NAD(P)(H) cycling assays were adapted from Gibon and Larher (1997). All reagents were from Sigma.  
21 *A. thaliana* plantlets were grown for seven days in continuous light (Benamar A, 2013) then challenged  
22 for 12 min. with flg22 (1  $\mu$ M) as previously described (Bisceglia & Savatin, 2015). Seedlings were  
23 harvested in pools of 80-100 mg each and immediately frozen in liquid nitrogen. Reduced and oxidised  
24 forms were extracted with 100 mM NaOH and 100 mM HCl respectively, and heated at 95°C for 5 min.  
25 After cooling down, tubes were centrifuged at 10,000 g for 10 min. Then 5  $\mu$ l of the supernatant were  
26 transferred to flat bottom polystyrene microplates (Greiner), neutralised with 5  $\mu$ l of 100 mM HCl



1 (reduced forms) or 100 mM NaOH (oxidised forms), and 90  $\mu$ l of determination mix added. For NAD(H)  
2 measurements, final concentrations of the reagents were 100 mM Tricine/KOH buffer, pH 9.0, 10 mM  
3  $MgCl_2$ , 8 mM EDTA, 1% v/v ethanol, 1 mM thiazolyl blue, 0.5 mM phenazine ethosulfate and 20  
4 units·ml<sup>-1</sup> alcohol dehydrogenase (Merck). For NADP(H) measurements, final concentrations of the  
5 reactants were 100 mM Tricine/KOH buffer, 10 mM  $MgCl_2$ , 8 mM EDTA, 5 mM glucose-6-phosphate,  
6 1 mM thiazolyl blue, 0.5 mM phenazine ethosulfate and 10 units·ml<sup>-1</sup> glucose-6-phosphate  
7 dehydrogenase grade I (Merck). Changes in absorbance were read at 570 nm in an MP96 reader  
8 (SAFAS) until stabilised. For each coenzyme form and/or each microplate a standards curve ranging  
9 from 0 to 40 pmol per well was used; blanks without enzyme were also recorded in order to subtract  
10 interferences coming from the extracts. Results are expressed as the average obtained for 3 independent  
11 extracts.

## 12 **Oxidative burst measurements**

13 *A. thaliana* plantlets were grown for 7 days in continuous light (Benamar et al., 2013) and immunity-  
14 related accumulation of H<sub>2</sub>O<sub>2</sub> following stimulation with flg22 (1  $\mu$ M) was analyzed as previously  
15 described (Bisceglia & Savatin, 2015). The purity of the flg22 peptide (synthesized by GENECUST,  
16 Boynes, France) was estimated at 96.14%. Luminescence measurements were performed with a  
17 microplate reader SPARK 10M (TECAN) using 96-well microtiter plates (flat bottom, white, Greiner).  
18 For each plant type, results are expressed as the average luminescence obtained for 4 wells (*i.e.*, 120  
19 plantlets).

## 20 **Molecular Phylogenetic analysis by the Maximum Likelihood method**

21 Protein sequences of NADKc-like proteins were retrieved from the Phytozome website (Goodstein et  
22 al., 2012), with some exceptions. The sequences of *U. mutabilis* and *C. braunii* were retrieved from the  
23 ORCAE project website (Sterck et al., 2012) and those of *S. minuta*, *E. fimbriata*, *Mougeotia* sp. and  
24 *Spirogyra* sp. were retrieved from the One KP project website (Matasci et al., 2014). The evolutionary  
25 history of NADKc was inferred by using the Maximum Likelihood method, based on the JTT matrix-  
26 based model (Jones et al., 1992). The tree with the highest log-likelihood (-31386.44) is shown. The

1 percentage of trees produced in which the associated taxa clustered together is shown next to the  
2 branches. Initial tree(s) for the heuristic search were obtained automatically by applying Neighbor-Join  
3 and BioNJ algorithms to a matrix of pairwise distances estimated using a JTT model, and then selecting  
4 the topology with the highest log-likelihood value. A discrete Gamma distribution was used to model  
5 evolutionary rate differences between sites (5 categories (+G, parameter = 0.9891)). The tree is drawn  
6 to scale, with branch lengths based on the number of substitutions per site. The analysis involved 45  
7 amino acid sequences. There were a total of 1196 positions in the final dataset. Evolutionary analyses  
8 were performed in MEGA7 (Kumar et al., 2016).

9

## 10 Supplemental references

- 11 **Benamar A, Pierart A, Baecker V, Avelange-Macherel M, Rolland A, Gaudichon S, di Gioia**  
12 **L, Macherel, D** (2013) Simple system using natural mineral water for high-throughput phenotyping of  
13 *Arabidopsis thaliana* seedlings in liquid culture. *International Journal of High Throughput Screening* **4**:  
14 1-15
- 15 **Bisceglia NG, Gravino M, Savatin DV** (2015) Luminol-based Assay for Detection of Immunity  
16 Elicitor-induced Hydrogen Peroxide Production in *Arabidopsis thaliana* Leaves. *BioProtocols* **5**: 1-7
- 17 **Casabona M, Vandenbrouck Y, Attree I, and Couté Y** (2013) Proteomic characterization of  
18 *Pseudomonas aeruginosa* PAO1 inner membrane. *Proteomics* **13**: 2419-2423
- 19 **Dell'Aglio E, Giustini C, Salvi D, Brugière S, Delpierre F, Moyet L, Baudet M, Seigneurin-**  
20 **Berny D, Matringe M, Ferro M, et al** (2013<sup>a</sup>) Complementary biochemical approaches applied to the  
21 identification of plastidial calmodulin-binding proteins. *Mol Biosyst* **9**: 1234-1248
- 22 **Dell'Aglio E** (2013<sup>b</sup>) The regulation of plastidial proteins by calmodulins. Université de Grenoble
- 23 **Elledge SJ, Mulligan JT, Ramer SW, Spottswood M, Davis RW** (1991) Lambda YES: a  
24 multifunctional cDNA expression vector for the isolation of genes by complementation of yeast and  
25 *Escherichia coli* mutations. *Proc Natl Acad Sci USA* **88**: 1731-1735
- 26 **Gibon Y, Larher F** (1997) Cycling assay for nicotinamide adenine dinucleotides: NaCl precipitation  
27 and ethanol solubilization of the reduced tetrazolium. *Analytical Biochemistry* **251**: 153-157
- 28 **Goodstein DM, Shu SQ, Howson R, Neupane R, Hayes RD, Fazo J, Mitros T, Dirks W, Hellsten**  
29 **U, Putnam N, et al** (2012) Phytozome: a comparative platform for green plant genomics. *Nucleic Acids*  
30 *Research* **40**: D1178-D1186
- 31 **Jones D, Taylor W, Thornton J** (1992) The rapid generation of mutation data matrices from protein  
32 sequences. *Comput Appl Biosci* **8**: 275-282
- 33 **Karimi M, Depicker A, Hilson P** (2007) Recombinational cloning with plant Gateway vectors.  
34 *Plant Physiol* **145**: 1144-1154
- 35 **Kumar S, Stecher G, Tamura K** (2016) Molecular evolutionary genetics analysis version 7.0 for  
36 bigger datasets. *Mol Biol Evol* **33**
- 37 **Matasci N, Hung LH, Yan ZX, Carpenter EJ, Wickett NJ, Mirarab S, Nguyen N, Warnow T,**  
38 **Ayyampalayam S, Barker M, et al** (2014) Data access for the 1,000 Plants (1KP) project. *Gigascience*  
39 **3**
- 40 **Michaud M, Ubrig E, Filleur S, Erhardt M, Ephritikhine G, Maréchal-Drouard L, Duchêne**  
41 **A-M** (2014) Differential targeting of VDAC3 mRNA isoforms influences mitochondria morphology.  
42 *Proc Natl Acad Sci USA* **111**: 8991-8996
- 43 **Murashige T, Skoog F** (1962) A revised medium for rapid growth of bioassays with tobacco tissue  
44 culture. *Physiol Plant* **15**: 473-497
- 45 **Scopes RK** (1974) Measurement of protein by spectroscopy at 205 nm. *Anal. Biochem.* **59**: 277-282

1 Sun Y, Li L, Macho AP, Han Z, Hu Z, Zipfel C, Zhou JM, Chai J. (2013) Structural basis for  
2 flg22-induced activation of the Arabidopsis FLS2-BAK1 immune complex. *Science* **342**: 624-8

3 Sterck L, Billiau K, Abeel T, Rouze P, van de Peer Y (2012) ORCAE: online resource for  
4 community annotation of eukaryotes. *Nature Methods* **9**: 1041-1041

5 Turner WL, Waller JC, Vanderbeld B, Snedden WA (2004) Cloning and characterization of two  
6 NAD kinases from Arabidopsis. Identification of a calmodulin binding isoform. *Plant Physiol* **135**:  
7 1243-1255  
8

## 9 Supplemental Figures Legend

10 **Supplementary Figure S1.** CaM-affinity purification of native CaM-dependent NAD<sup>+</sup> kinase from  
11 Arabidopsis plantlets. Proteins loaded and eluted from the CaM affinity chromatography column were  
12 separated by SDS-PAGE and stained with silver nitrate. In the “Loaded fraction”, 24 µg in 38 µl were  
13 loaded; in the washings and EGTA elution fractions, 38 µl of each fraction were loaded (concentration  
14 not determined). Mass spectrometry-based proteomics was used to identify proteins strongly enriched  
15 in the EGTA elution compared to the Ca<sup>2+</sup>-containing washing steps (Supplemental Table S1). Protein  
16 bands analysed by mass spectrometry are included in red boxes.

17 **Supplementary Fig. S2.** Features of NADKc primary sequence and its homologues in other plant and  
18 algae species. (A) putative CaM binding site (*A. thaliana* NADKc amino acids 167-200). Red residues  
19 are those constituting the 1-5-8-14 motif. This domain is not conserved in *C. subellipsoidea*, *U. mutabilis*  
20 and *S. minuta*. *A. thaliana*: *Arabidopsis thaliana*, *S. phallax*: *Sphagnum phallax*, *P. patens*:  
21 *Physcomitrella patens*, *M. polymorpha*: *Marchantia polymorpha*, *S. mollendorffii*: *Selaginella*  
22 *mollendorffii*, *S. lycopersicum*: *Solanum lycopersicum*, *G. max*: *Glycine max*, *M. truncatula*: *Medicago*  
23 *truncatula*, *P. trichocarpa*: *Populus trichocarpa*, *M. acuminata*: *Musa acuminata*, *O. sativa*: *Oryza*  
24 *sativa*, *B. distachyon*: *Brachypodium distachyon*, *S. italica*: *Setaria italica*, *Z. mays*: *Zea mays*, *C.*  
25 *subellipsoidea*: *Coccomyxa subellipsoidea*, *U. mutabilis*: *Ulva mutabilis*, *S. minuta*: *Spirotaenia minuta*,  
26 *K. flaccidum*: *Klebsormidium flaccidum*, *E. fimbriata*: *Entransia fimbriata*. (B) Walker A motif (in red,  
27 residues characterizing the motif; *A. thaliana* NADKc amino acids 236-250). For gene references, see  
28 the legend of Fig. S6.

29 **Supplementary Fig. S3.** Purification of recombinant NADKc produced in *E. coli*. 6HIS-Δ38NADKc  
30 was purified as indicated in Material and Methods. Lane 1: Rosetta2 soluble extract transformed with  
31 empty pET28a (40 µg); lane 2: Rosetta2 soluble extract transformed with pET28a6HIS-Δ38NADKc (40

1  $\mu\text{g}$ ); lane 3: Ni-NTA pool (10  $\mu\text{g}$ ); lane 4: urea-denatured 6HIS- $\Delta$ 38NADKc purified on Ni-NTA (10  
2  $\mu\text{g}$ ); lane 5: refolded 6HIS- $\Delta$ 38NADKc (2  $\mu\text{g}$ ).

3 **Supplementary Fig. S4.** NADK<sub>cNter</sub>-YFP associates with mitochondria in tobacco leaves.  
4 Representative pictures of transiently transformed tobacco leaf cells. Left: YFP (green), Center: RFP  
5 (red), and Right: merged fluorescence. The top row shows a representative image of tobacco cells co-  
6 transformed with the NADK<sub>cNter</sub>-YFP construct and a mitochondrial marker, pSu9-RFP. The middle  
7 row shows a close-up of mitochondria from the lower right region of the images in the top row (white  
8 boxes). White arrows indicate regions in which the YFP signal appears peripheral with respect to the  
9 RFP signal. The bottom row shows a representative image of tobacco cells transformed with the YFP-  
10 NADKc construct alone. The central image shows the background signal in the RFP channel. White  
11 bars represent 2  $\mu\text{m}$  in the upper and middle row, and 10  $\mu\text{m}$  in the lower row.

12 **Supplementary Fig. S5.** Phenotype of *nadkc* mutants. (A) 21-day-old plants grown under long day  
13 photoperiod (16 h light/8 h dark); (B) 28-day-old plants grown under short day photoperiod (8 h light/16  
14 h dark). (C-E) Photosynthetic parameters in Col-0 and *nadkc* plants: (C) NPQ, (D) Fv/Fm and (E)  
15 electron transport rate.

16 **Supplementary Fig. S6.** Phylogeny of NADKc. Maximum likelihood phylogenetic tree of NADKc-  
17 like proteins in the following plant and algal species: *Arabidopsis thaliana* (*A. thaliana*), *Populus*  
18 *trichocarpa* (*P. trichocarpa*), *Manihot esculenta* (*M. esculenta*), *Gossypium raimondii* (*G. raimondii*),  
19 *Solanum lycopersicum* (*S. lycopersicum*), *Setaria italica* (*S. italica*), *Zea mays* (*Z. mays*), *Oryza sativa*  
20 (*O. sativa*), *Brachypodium distachyon* (*B. distachyon*), *Musa acuminata* (*M. acuminata*), *Marchantia*  
21 *polymorpha* (*M. polymorpha*), *Physcomitrella patens* (*P. patens*), *Sphagnum phallax* (*S. phallax*),  
22 *Selaginella mollendorffii* (*S. mollendorffii*), *Klebsormidium flaccidum* (*K. flaccidum*), *Coccomyxa*  
23 *subellipsoidea* (*C. subellipsoidea*), *Ulva mutabilis* (*U. mutabilis*), *Spirotaenia minuta* (*S. minuta*),  
24 Mougeotia sp., Spirogyra sp. and *Entransia fimbriata* (*E. fimbriata*). Accession numbers: *A. thaliana*-1  
25 (NADKc): At1g04280, *A. thaliana*-2: At1g06750, *A. thaliana*-3: At2g30630, *P. trichocarpa*-1:  
26 Potri.008G162000, *P. trichocarpa*-2: Potri.002G043000, *P. trichocarpa*-3: Potri.005G220000, *P.*  
27 *trichocarpa*-4: Potri.008G162400, *M. esculenta*-1: Manes.15G036900, *M. esculenta*-2:  
28 Manes.03G168900, *M. esculenta*-3: Manes.01G200600, *M. esculenta*-4: Manes.05G086200, *G.*

1 *raimondii-1*: Gorai.011G171100, *G. raimondii-2*: Gorai.006G246600, *G. raimondii-3*:  
2 Gorai.004G074100, *G. raimondii-4*: Gorai.013G104300, *S. lycopersicum-1*: Solyc06g053810, *S.*  
3 *lycopersicum-2*: Solyc06g031670, *S. lycopersicum-3*: Solyc08g059750, *S. italica-1*: Seita.9G163700, *S.*  
4 *italica-2*: Seita.3G185100, *S. italica-3*: Seita.5G337000, *Z. mays-1*: GRMZM2G070252, *Z. mays-2*:  
5 GRMZM2G368410, *O. sativa-1*: Os03g43010, *O. sativa-2*: Os05g43300, *O. sativa-3*: Os01g56764, *B.*  
6 *distachyon-1*: Bradi1g14307, *B. distachyon-2*: Bradi2g51490, *B. distachyon-3*: Bradi2g20400, *M.*  
7 *acuminata-1*: SMUA\_Achr5T03210, *M. acuminata-2*: GSMUA\_Achr7T01560, *M. polymorpha*:  
8 Mapoly0142s0012, *P. patens*: Pp3c2\_3490V3, *S. phallax-1*: Sphallax0059s0037, *S. phallax-2*:  
9 Sphallax0011s0002, *S. phallax-3*: Sphallax0120s0019, *S. mollendorffii-1*: scaffold 73427, *S.*  
10 *mollendorffii-2*: scaffold 231175, *K. flaccidum*: kfl00274\_0130, *C. subellipsoidea*: XP\_005648203, *U.*  
11 *mutabilis*: UM028\_0076.1, *S. minuta*: NNHQ\_2000691, *Mougeotia*: ZRMT\_2002068, *Spirogyra*:  
12 HAOX\_2025158, *E. fimbriata*: BFIK\_2025349. The tree is drawn to scale, with branch lengths  
13 measured in the number of substitutions per site (scale bar in the bottom-left corner). The numbers at  
14 the interior nodes are bootstrap percentages.

15 **Supplementary Table S1.** List of Arabidopsis proteins bound on CaM-affinity column in the presence  
16 of Ca<sup>2+</sup> and eluted by EGTA identified by mass-spectrometry.

17 **Supplementary Table S2.** Primers used in this study.

18

19

20 **Table 1: NADKc kinetic parameters**

Substrate varied	Constant substrate	K <sub>M</sub> (μM)	k <sub>cat</sub> (s <sup>-1</sup> )	k <sub>cat</sub> /K <sub>M</sub> (μM <sup>-1</sup> .s <sup>-1</sup> )
ATP	NAD <sup>+</sup> (10 mM)	203(±30)	41(±2)	0.2
CTP	NAD <sup>+</sup> (10 mM)	283(±70)	42(±1)	0.15
GTP	NAD <sup>+</sup> (10 mM)	522(±135)	26(±1)	0.05
UTP	NAD <sup>+</sup> (10 mM)	207(±26)	29.5(±2)	0.14
NAD <sup>+</sup>	ATP (8 mM)	147 (±17)	42(±2)	0.28
NADH <sup>+</sup>	ATP (8 mM)	n.d.	n.d.	n.d.
NAAD <sup>+</sup>	ATP (8 mM)	n.d.	n.d.	n.d.

21 n.d.: not detected

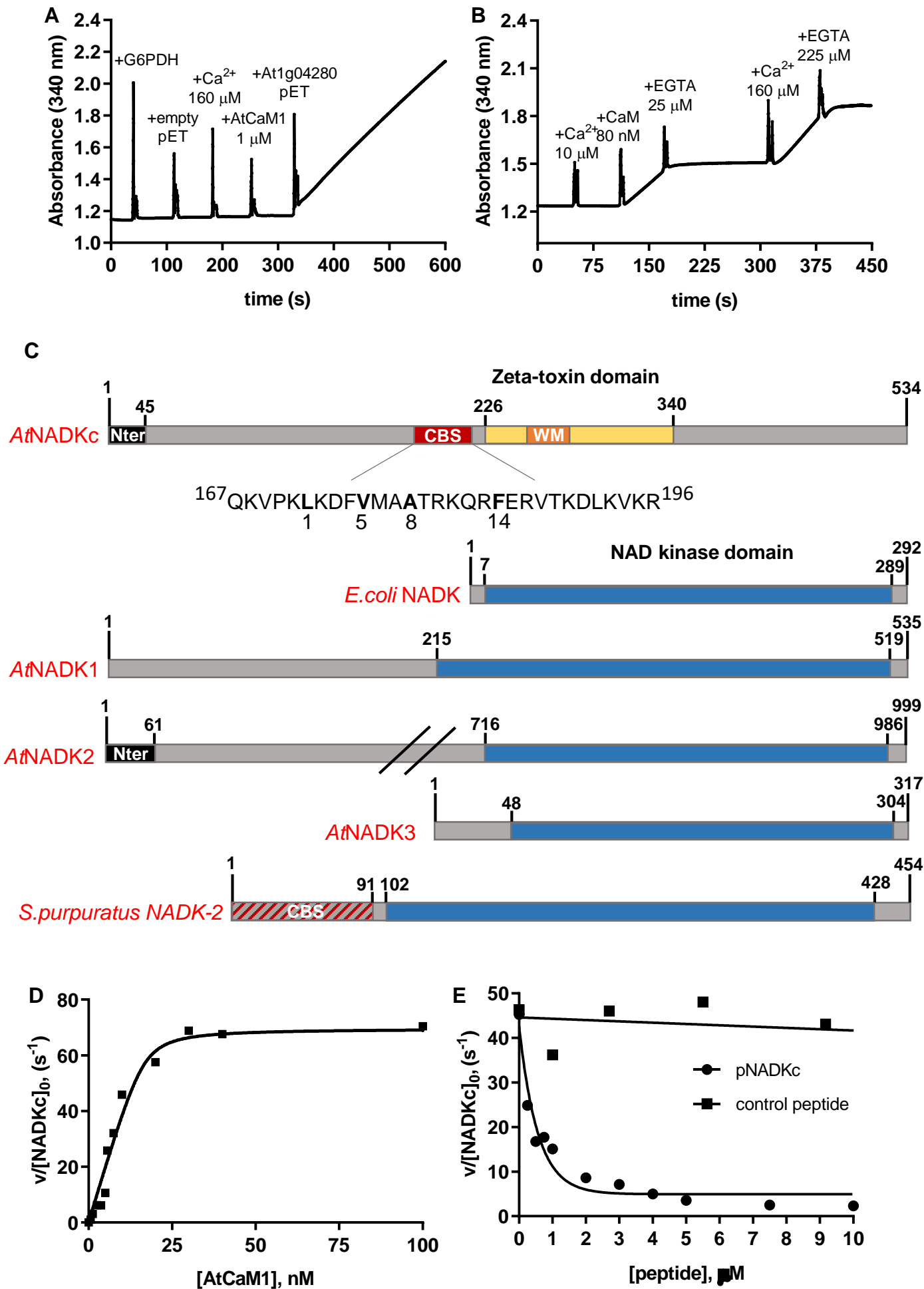
22

1

2 **Table 2: Comparison of CaM-dependent NADK activity in different photosynthetic organisms.**

	<i>A. thaliana</i>	<i>M. polymorpha</i>	<i>K. flaccidum</i>	<i>C. reinhardtii</i>
<b>Total activity<sup>a</sup></b>	31.2(±2.8)	6.9(±0.7)	5.8(±0.3)	24.6(±1.4)
<b>CaM/Ca<sup>2+</sup> - independent activity<sup>b</sup></b>	1.0(±0.3)	1.0(±0.1)	1.8(±0.3)	29.7(±2.7)
<b>CaM/Ca<sup>2+</sup> - dependent activity<sup>c</sup></b>	30.2	5.9	4.0	n.d.

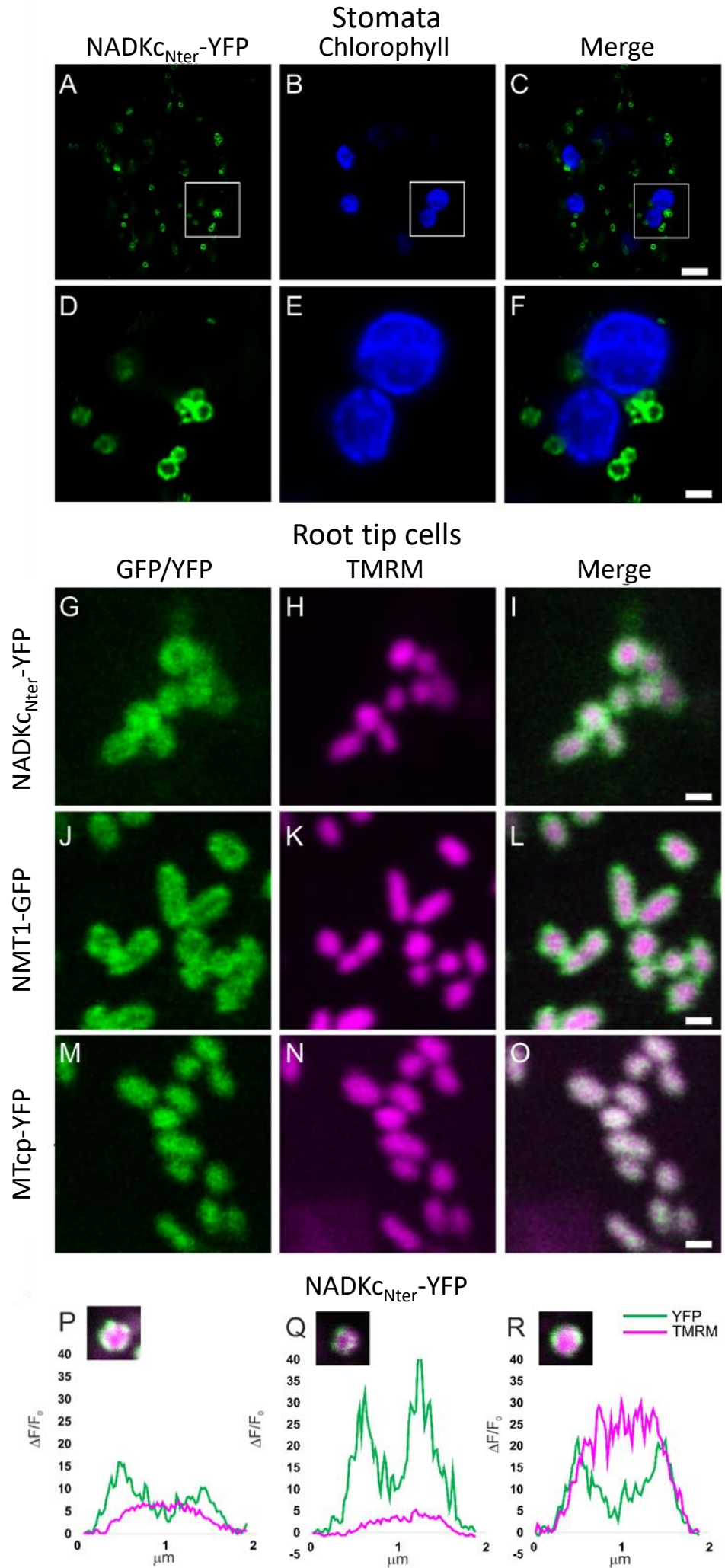
3 n.d.: not detected.

**Figure 1**

**Figure 1.** Biochemical properties of a CaM-dependent NAD<sup>+</sup> kinase identified in Arabidopsis. (A) NAD<sup>+</sup> kinase activity measured in an *E. coli* extract expressing an empty pET28b(+) and an *E. coli* extract expressing At1g04280. Spikes correspond to the moments of addition of glucose 6-phosphate dehydrogenase (G6PDH), Ca<sup>2+</sup>, AtCaM1, and *E. coli* extracts (10 μg). (B) NAD<sup>+</sup> kinase activity in an *E. coli* bacterial extract expressing At1g04280. Ca<sup>2+</sup>, AtCaM1 and EGTA were added at different times, as indicated in the graph. (C) Schematic representation of the NADKc primary sequence and comparison with previously known NAD<sup>+</sup> kinases. Yellow: zeta-toxin domain (InterPro Homologous superfamily: IPR010488); black: N-terminal region with putative organelle target sequence; red: putative conserved Type A 1-8-14 CaM-binding site (detailed below the scheme); orange: Walker A motif (ATP-binding site); blue: NAD<sup>+</sup> kinase domain (InterPro Homologous Superfamily: IPR016064); red/grey: N-terminal sequence expected to contain a CaM-binding site according to Love et al, 2015. Sequences used for comparison (UniProt): *E. coli* NAD<sup>+</sup> kinase: P0A7B3; *A. thaliana* NAD<sup>+</sup> kinases: AtNADK1: Q56YN3; AtNADK2: Q9C5W3; AtNADK3: Q500Y9; *Strongylocentrotus purpuratus* NAD<sup>+</sup> kinase-2 (sea urchin CaM-dependent NAD<sup>+</sup> kinase, Love et al., 2015): C3RSF7. (D) Affinity of NADKc recombinant protein for AtCaM1: Activity of the purified NADKc recombinant protein after denaturation in urea and subsequent refolding was measured in the presence of 50 μM Ca<sup>2+</sup> and as a function of [AtCaM1]. Experiments were performed in triplicate and data shown are from one representative experiment. Binding data were analysed assuming tight binding. K<sub>d</sub> value for AtCaM1 binding varied from 0.6 to 1 nM. (E) Inhibition of NADKc activity by competition with the putative CaM-binding site (black dots). Black squares correspond to results obtained with a negative control peptide, which does not bind AtCaM1.

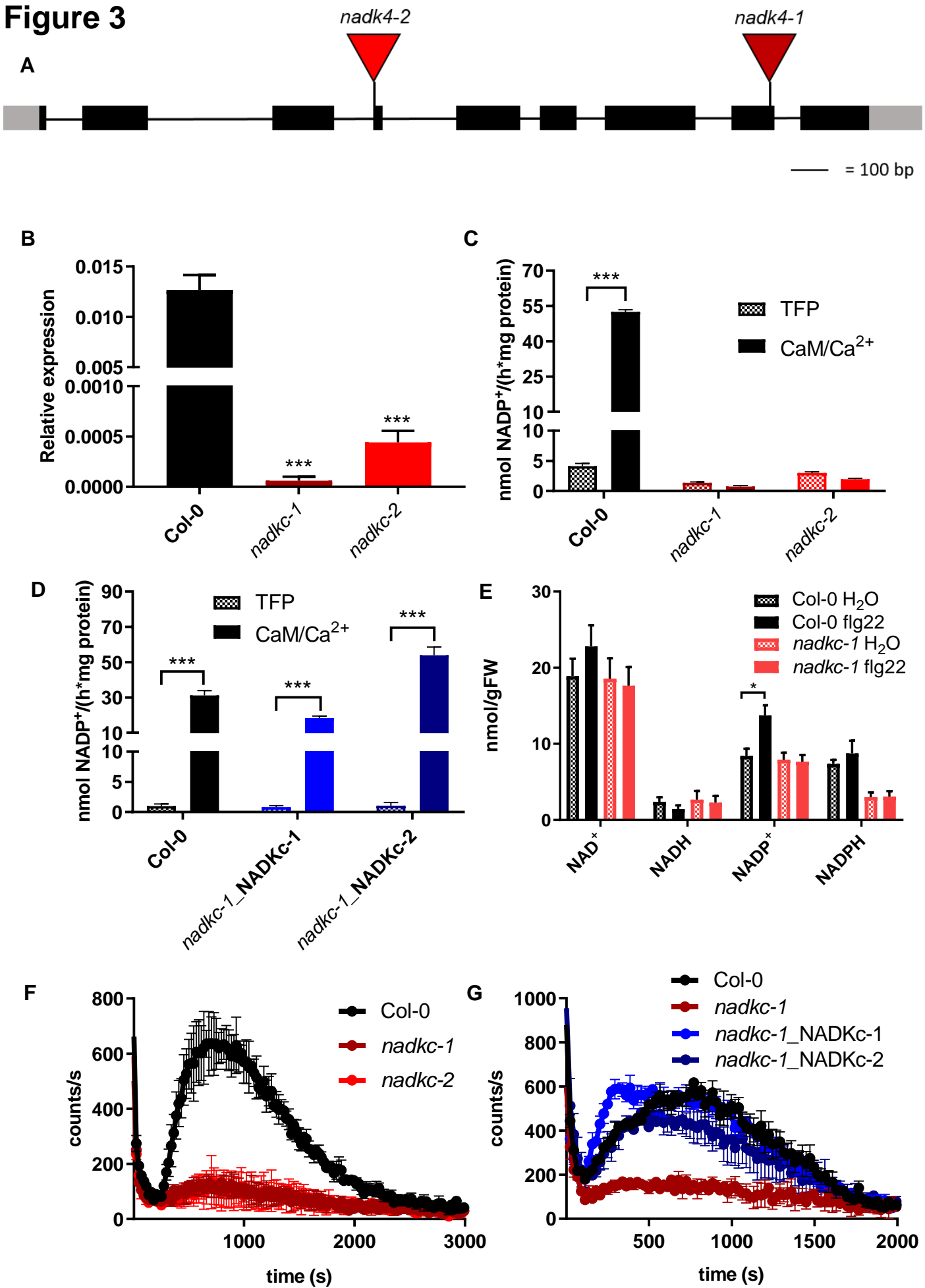


**Figure 2**



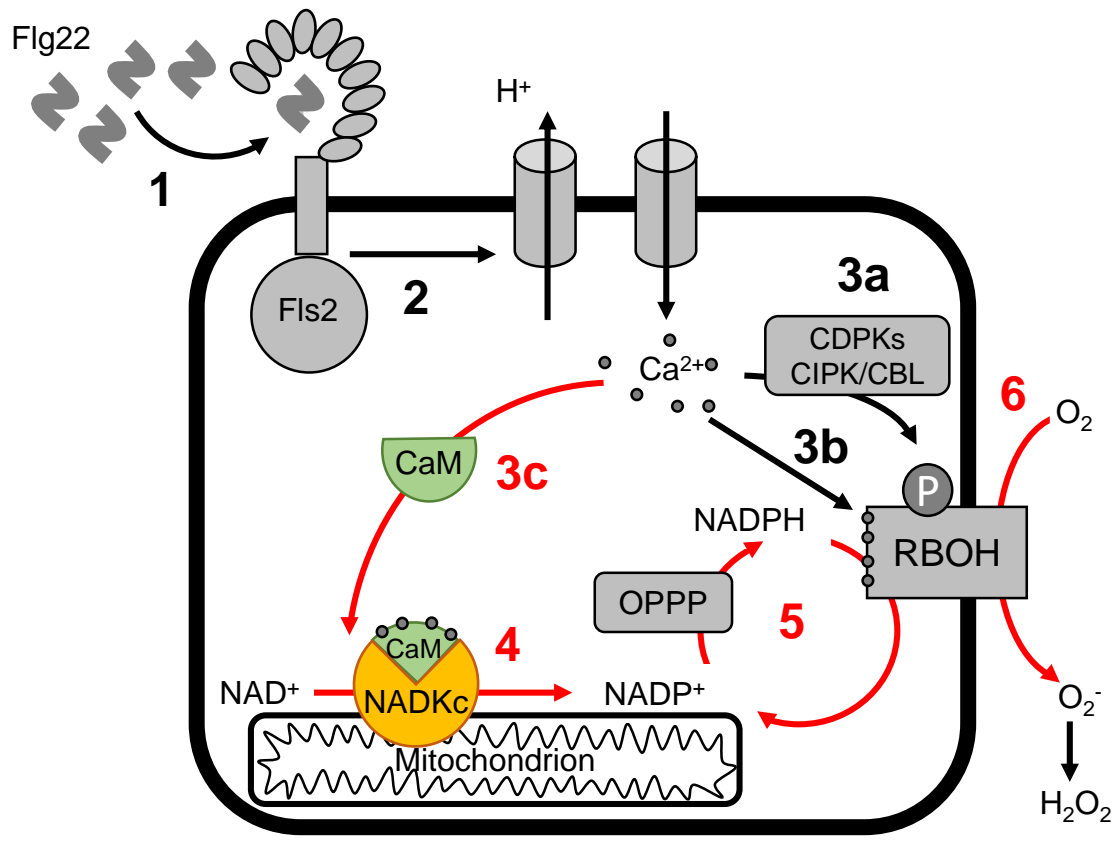
**Figure 2.** Analysis of submitochondrial localization of NADKc<sub>Nter</sub>-YFP. (A to C) Confocal laser scanning microscopy images from stomata guard cells of a representative Arabidopsis seedling stably expressing NADKc<sub>Nter</sub>-YFP. Scale bar = 5  $\mu$ m. (D to E) Higher magnification of the region of interest shown in A to C (white squares). Scale bar = 1  $\mu$ m. (A, D) YFP fluorescence in green; (B, E) chlorophyll fluorescence in blue; (C, F) merge between YFP and chlorophyll fluorescences. (G to I) Confocal laser scanning microscopy images from root tip cells of a representative Arabidopsis seedling stably expressing NADKc<sub>Nter</sub>-YFP and stained with the mitochondrial matrix marker TMRM. Scale bar = 1  $\mu$ m. (J to L) Confocal laser scanning microscopy images from root tip cells of a representative Arabidopsis seedling stably expressing NMT-GFP and stained with the mitochondrial matrix marker TMRM. Scale bar = 1  $\mu$ m. (M to O) Confocal laser scanning microscopy images from root tip cells of a representative Arabidopsis seedling stably expressing MT-cpYFP and stained with the mitochondrial matrix marker TMRM. Scale bar = 1  $\mu$ m. (G, M) YFP fluorescence in green; (J) GFP fluorescence in green; (H, K and N) TMRM fluorescence in magenta; (I, L and O) merge between YFP/GFP and TMRM fluorescences. NMT1-GFP and MT-cpYFP were used as markers for the mitochondrial outer mitochondrial membrane (OMM) and matrix, respectively. (P to R) Normalized pixel intensity distributions in the YFP and TMRM fluorescence channels plotted centrally across three individual mitochondria of a seedling expressing the NADKc<sub>Nter</sub>-YFP.

**Figure 3**



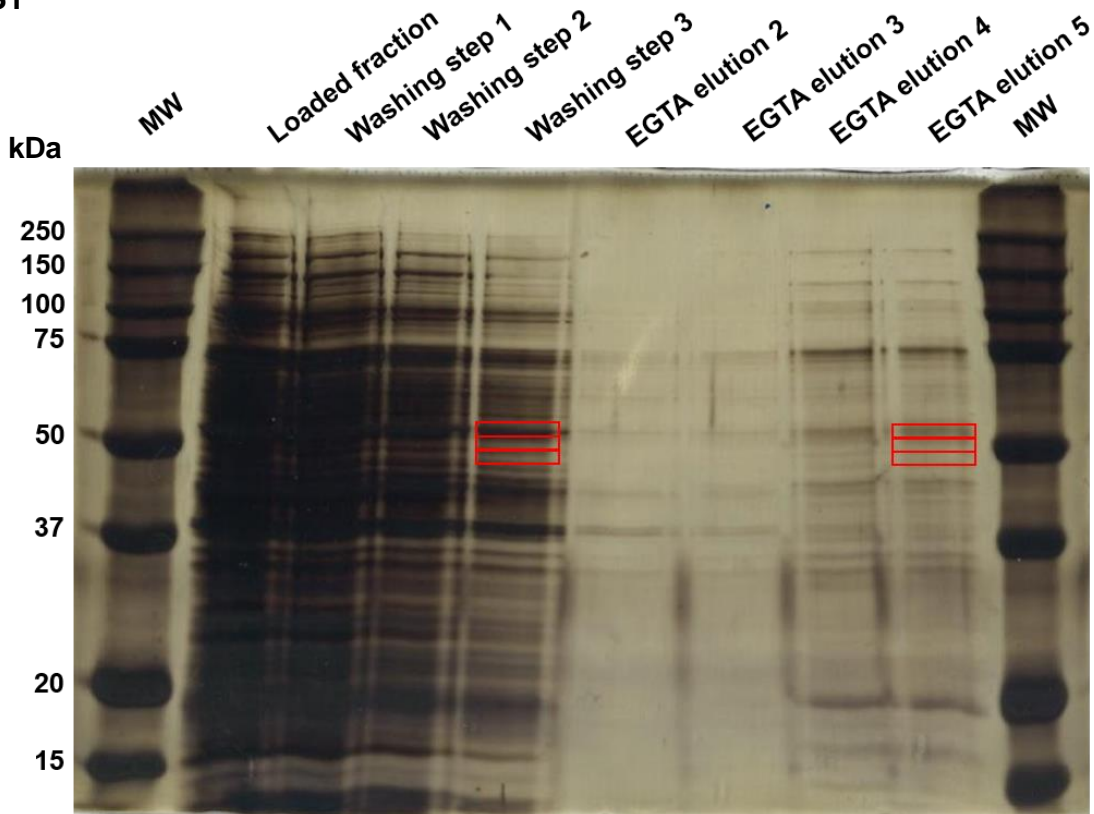
**Figure 3.** The CaM/Ca<sup>2+</sup>-dependent NAD<sup>+</sup> kinase activity of Arabidopsis seedlings is absent in *nadkc* mutants. (A) schematic representation of the NADKc gene and position of the T-DNA insertions in the *nadkc-1* and *nadkc-2* mutant lines. (B) NADKc transcript levels in Col-0 and *nadkc*-mutant seedlings. Levels are expressed relative to GAPDH. Data shown correspond to mean +/- s.d., n=3. (C) NAD<sup>+</sup> kinase activity measured in Col-0 and *nadkc* mutant plants (7-day-old whole plantlets), in the presence of the CaM inhibitor TFP (40 μM) or AtCaM1 (250 nM) and Ca<sup>2+</sup> (0.5 mM). Values correspond to the average of four replicates. (D) NAD<sup>+</sup> kinase activity measured in Col-0 and mutant plants complemented with NADKc gene (*nadkc-1\_NADKc-1* and *nadkc-1\_NADKc-2*) in 7-day-old whole plantlets, in the presence of the CaM inhibitor TFP (40 μM) or of AtCaM1 (250 nM) and Ca<sup>2+</sup> (0.5 mM). (E) NAD(P)<sup>+</sup> and NAD(P)H concentrations in 7-day-old seedlings exposed (flg22, 1 μM) or unexposed (H<sub>2</sub>O) for 12 min. to the bacterial elicitor flagellin22. (80-100 mg of tissue per measure, data shown correspond to mean +/- s.e.m. for 3 biological replicates). (F) Flg22 (1 μM)-induced oxidative burst in 7-day-old Col-0 and *nadkc* mutant seedlings (30 plantlets per well, data shown correspond to mean +/- s.d. for 4 wells). (G) Flg22 (1 μM)-induced oxidative burst in Col-0, *nadkc-1* mutant and mutant plants complemented with NADKc gene (*nadkc-1\_NADKc-1* and *nadkc-1\_NADKc-2*); 7-day-old seedlings, 30 plantlets per well. Data shown correspond to mean +/- s.d. for 4 wells. Asterisks indicate a significant difference between two conditions based on a Welch's t test (\*p < 0.05; \*\*\*p < 0.001).

Figure 4



**Figure 4.** Hypothetical model of the role of CaM/Ca<sup>2+</sup>-dependent NADKc in sustaining the flg22-induced oxidative burst in Arabidopsis seedlings. Numbers refer to known sequential events; red numbers highlight events related to NADKc activation: 1. binding of Flg22 elicitor to the Fls2 receptor (Sun et al., 2013); 2. activation of proton efflux and Ca<sup>2+</sup> influx; 3a. Ca<sup>2+</sup>-dependent activation of CDPKs and CIPK/CBLs that phosphorylate RBOH proteins; 3b. Ca<sup>2+</sup> binding to RBOH proteins; 3c. Ca<sup>2+</sup> binding to CaM, leading to CaM structural modification and formation of the CaM/NADKc complex; 4. activation of NADP<sup>+</sup> production by NADKc; 5. increased flux in the oxidative pentose phosphate pathway (OPPP), leading to a higher availability of NADPH; 6. production of the extracellular oxidative burst by NADPH oxidases (RBOH proteins).

Figure S1



**Supplemental Figure S1.** CaM-affinity purification of native CaM-dependent NAD<sup>+</sup> kinase from Arabidopsis plantlets. Proteins loaded and eluted from the CaM affinity chromatography column were separated by SDS-PAGE and stained with silver nitrate. In the “Loaded fraction”, 24  $\mu$ g in 38  $\mu$ l were loaded; in the washings and EGTA elution fractions, 38  $\mu$ l of each fraction were loaded (concentration not determined). Mass spectrometry-based proteomics was used to identify proteins strongly enriched in the EGTA elution compared to the Ca<sup>2+</sup>-containing washing steps (Supplemental Table S1). Protein bands analysed by mass spectrometry are included in red boxes.

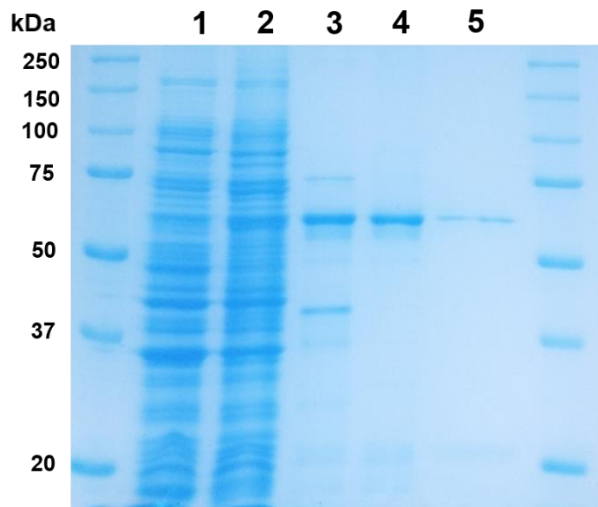
**Figure S2****A****Predicted CaM-binding site****B****Walker A motif**

<i>A. thaliana-1</i> (At1g04280 - NADKc)	167	QKVPK <b>L</b> KDF <b>V</b> MA <b>A</b> TRK <b>Q</b> R <b>F</b> ERVTKDLK <b>V</b> KR	196	236	MG <b>G</b> GM <b>G</b> AG <b>K</b> STVL <b>K</b> D	250
<b>Plants</b>						
<i>S. phfallax-1</i>		--Q <b>K</b> R <b>L</b> R <b>K</b> A <b>V</b> W <b>L</b> A <b>T</b> R <b>P</b> Q <b>R</b> I <b>E</b> R <b>V</b> L <b>K</b> C <b>L</b> K <b>T</b> K <b>R</b>			I <b>G</b> G <b>G</b> M <b>G</b> AG <b>K</b> ST <b>V</b> V <b>Q</b> E	
<i>P. patens</i>		--E <b>K</b> K <b>L</b> H <b>K</b> A <b>V</b> L <b>C</b> A <b>L</b> K <b>K</b> Q <b>R</b> <b>Y</b> E <b>A</b> V <b>L</b> K <b>S</b> L <b>S</b> T <b>K</b> R			I <b>G</b> G <b>G</b> M <b>G</b> AG <b>K</b> ST <b>I</b> V <b>K</b> E	
<i>M. polymorpha</i>		-Q <b>K</b> R <b>S</b> L <b>K</b> K <b>A</b> V <b>L</b> S <b>A</b> T <b>R</b> K <b>Q</b> R <b>Y</b> Q <b>R</b> V <b>M</b> Q <b>D</b> L <b>K</b> T <b>K</b> R			I <b>G</b> G <b>G</b> M <b>G</b> AG <b>K</b> ST <b>V</b> V <b>K</b> E	
<i>S. mollendorffii-1</i>		----N <b>L</b> R <b>S</b> I <b>V</b> MA <b>A</b> TRK <b>H</b> R <b>F</b> Q <b>R</b> A <b>M</b> Q <b>T</b> L <b>K</b> A <b>K</b> R			M <b>G</b> G <b>G</b> M <b>G</b> AG <b>K</b> ST <b>V</b> L <b>K</b> D	
<i>S. lycopersicum-1</i>		--Q <b>K</b> R <b>L</b> K <b>D</b> L <b>V</b> LA <b>A</b> TRK <b>Q</b> R <b>F</b> E <b>K</b> I <b>T</b> K <b>D</b> L <b>K</b> V <b>T</b> R			M <b>G</b> G <b>G</b> M <b>G</b> AG <b>K</b> ST <b>V</b> L <b>K</b> D	
<i>G. max-1</i>		-Q <b>K</b> K <b>K</b> L <b>K</b> G <b>I</b> L <b>L</b> A <b>A</b> T <b>R</b> E <b>Q</b> R <b>F</b> D <b>R</b> V <b>T</b> K <b>N</b> L <b>K</b> V <b>T</b> R			M <b>G</b> G <b>G</b> M <b>G</b> AG <b>K</b> ST <b>V</b> L <b>K</b> D	
<i>M. esculenta-1</i>		-K <b>R</b> H <b>K</b> L <b>K</b> D <b>V</b> V <b>L</b> A <b>A</b> TRK <b>Q</b> R <b>F</b> ER <b>V</b> N <b>K</b> E <b>L</b> K <b>V</b> T <b>R</b>			M <b>G</b> G <b>G</b> M <b>G</b> AG <b>K</b> ST <b>V</b> I <b>K</b> D	
<i>P. trichocarpa-1</i>		-K <b>K</b> P <b>K</b> L <b>K</b> G <b>I</b> V <b>MA</b> A <b>T</b> R <b>K</b> Q <b>R</b> <b>F</b> ER <b>V</b> T <b>K</b> N <b>L</b> K <b>V</b> T <b>R</b>			M <b>G</b> G <b>G</b> M <b>G</b> AG <b>K</b> ST <b>V</b> T <b>K</b> D	
<i>M. acuminata-1</i>		-Q <b>K</b> M <b>K</b> L <b>K</b> N <b>F</b> V <b>ME</b> A <b>T</b> R <b>K</b> L <b>R</b> <b>F</b> ER <b>V</b> T <b>K</b> D <b>L</b> K <b>V</b> T <b>R</b>			M <b>G</b> G <b>G</b> M <b>G</b> AG <b>K</b> ST <b>V</b> L <b>K</b> E	
<i>O. sativa-1</i>		A <b>S</b> K <b>K</b> K <b>L</b> R <b>N</b> L <b>V</b> L <b>E</b> A <b>T</b> R <b>K</b> Q <b>R</b> <b>F</b> ER <b>V</b> T <b>R</b> D <b>L</b> K <b>V</b> T <b>R</b>			M <b>G</b> G <b>G</b> M <b>G</b> AG <b>K</b> ST <b>V</b> L <b>K</b> E	
<i>B. distachyon-1</i>		-T <b>R</b> K <b>K</b> L <b>R</b> N <b>L</b> V <b>L</b> E <b>A</b> T <b>R</b> K <b>Q</b> R <b>F</b> ER <b>V</b> T <b>R</b> D <b>L</b> K <b>V</b> T <b>R</b>			M <b>G</b> G <b>G</b> M <b>G</b> AG <b>K</b> ST <b>V</b> L <b>K</b> E	
<i>S. italica-1</i>		-S <b>T</b> K <b>K</b> L <b>R</b> N <b>V</b> F <b>ME</b> A <b>T</b> R <b>K</b> Q <b>R</b> <b>F</b> AR <b>V</b> T <b>R</b> D <b>L</b> K <b>V</b> T <b>R</b>			M <b>G</b> G <b>G</b> M <b>G</b> AG <b>K</b> ST <b>V</b> L <b>ME</b>	
<i>Z. mays-1</i>		-S <b>K</b> R <b>K</b> L <b>R</b> N <b>M</b> V <b>L</b> E <b>A</b> T <b>R</b> K <b>Q</b> R <b>F</b> ER <b>V</b> T <b>R</b> D <b>L</b> K <b>V</b> T <b>R</b>			M <b>G</b> G <b>G</b> M <b>G</b> AG <b>K</b> ST <b>V</b> L <b>K</b> E	
<b>Algae</b>						
<i>K. flaccidum</i>		-K <b>R</b> H <b>S</b> L <b>K</b> R <b>A</b> V <b>L</b> S <b>A</b> T <b>R</b> T <b>Q</b> R <b>Y</b> K <b>Q</b> L <b>L</b> R <b>S</b> L <b>G</b> P <b>Q</b> R			M <b>A</b> G <b>G</b> M <b>G</b> AG <b>K</b> ST <b>V</b> R <b>Q</b> E	
<i>E. fimbriata</i>		--K-S <b>L</b> K <b>G</b> A <b>V</b> L <b>R</b> A <b>T</b> R <b>T</b> H <b>R</b> <b>Y</b> E <b>R</b> L <b>V</b> T <b>A</b> L <b>G</b> S <b>Q</b> R			M <b>G</b> G <b>G</b> M <b>G</b> AG <b>K</b> ST <b>A</b> A <b>R</b> R	
<i>Mougeotia sp.</i>		-K <b>K</b> M <b>T</b> <b>F</b> K <b>A</b> A <b>V</b> R <b>K</b> A <b>T</b> S <b>I</b> Q <b>R</b> V <b>K</b> K <b>V</b> I <b>E</b> H <b>L</b> G <b>P</b> Q <b>R</b>			I <b>G</b> G <b>G</b> M <b>G</b> AG <b>K</b> ST <b>V</b> - <b>K</b> E	
<i>Spyrogyra sp.</i>		-R <b>L</b> -S <b>F</b> K <b>K</b> A <b>V</b> L <b>N</b> A <b>T</b> R <b>N</b> Q <b>R</b> <b>ME</b> K <b>I</b> M <b>T</b> N <b>F</b> K <b>T</b> Q <b>Q</b>			L <b>G</b> G <b>G</b> M <b>G</b> AG <b>K</b> ST <b>V</b> A <b>K</b> Q	
<i>C. subellipsoidea</i>		n.d.			L <b>G</b> G <b>G</b> M <b>A</b> AG <b>K</b> ST <b>V</b> R <b>E</b> I	
<i>U. mutabilis</i>		n.d.			L <b>G</b> G <b>G</b> M <b>A</b> AG <b>K</b> ST <b>S</b> V <b>R</b> N <b>E</b>	
<i>S. minuta</i>		n.d.			L <b>G</b> G <b>G</b> M <b>G</b> AG <b>K</b> ST <b>A</b> V <b>K</b> E	

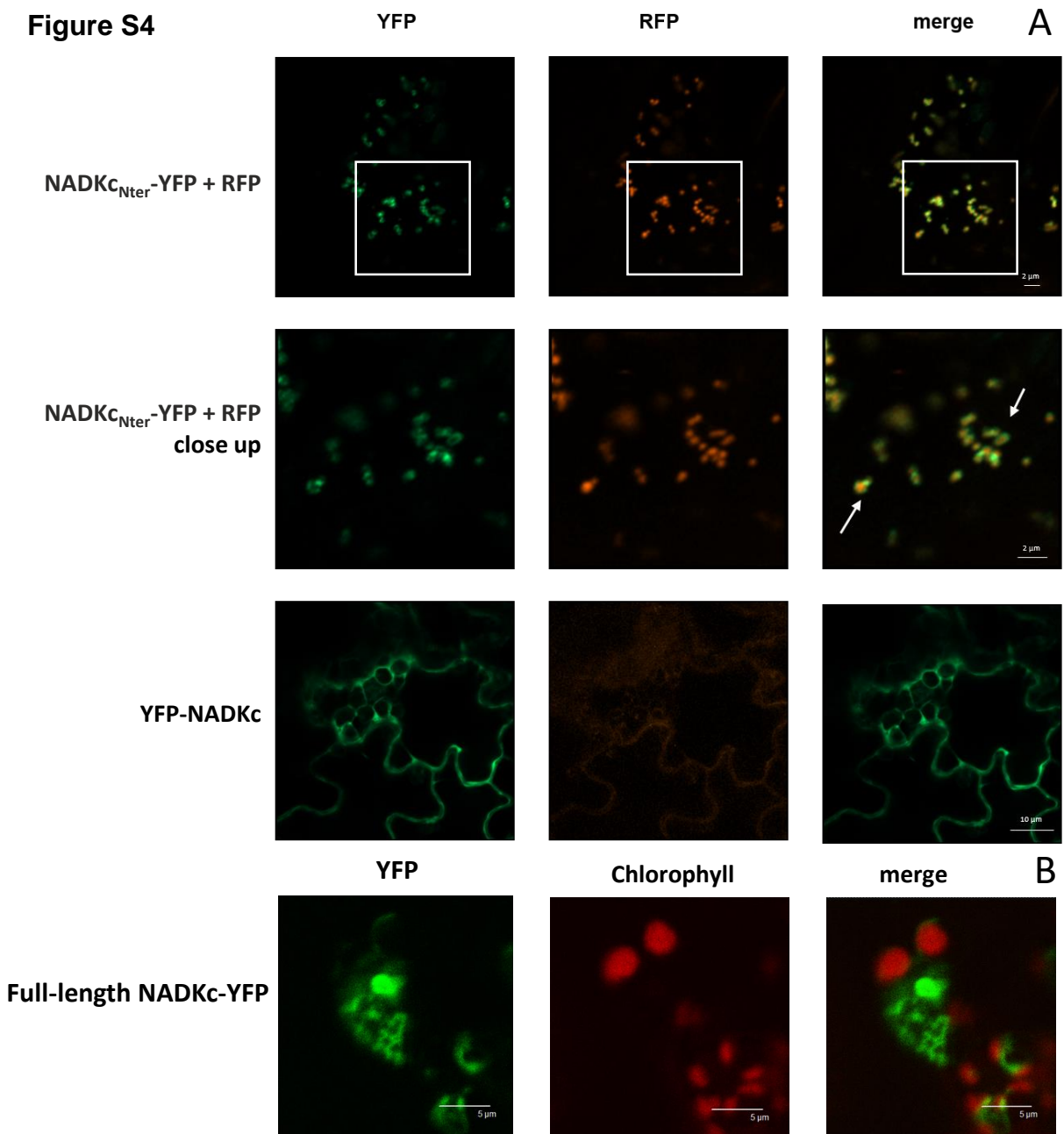
**Supplemental Figure S2.** Features of NADKc primary sequence and its homologues in other plant and algae species. (A) putative CaM binding site (Arabidopsis NADKc amino acids 167-200). Red residues are those constituting the 1-5-8-14 motif. This domain is not conserved in *C. subellipsoidea*, *U. mutabilis* and *S. minuta*. *A. thaliana*: *Arabidopsis thaliana*, *S. phallax*: *Sphagnum phallax*, *P. patens*: *Physcomitrella patens*, *M. polymorpha*: *Marchantia polymorpha*, *S. mollendorffii*: *Selaginella mollendorffii*, *S. lycopersicum*: *Solanum lycopersicum*, *G. max*: *Glycine max*, *M. truncatula*: *Medicago truncatula*, *P. trichocarpa*: *Populus trichocarpa*, *M. acuminata*: *Musa acuminata*, *O. sativa*: *Oryza sativa*, *B. distachyon*: *Brachypodium distachyon*, *S. italica*: *Setaria italica*, *Z. mays*: *Zea mays*, *C. subellipsoidea*: *Coccomyxa subellipsoidea*, *U. mutabilis*: *Ulva mutabilis*, *S. minuta*: *Spirotaenia minuta*, *K. flaccidum*: *Klebsormidium flaccidum*, *E. fimbriata*: *Entransia fimbriata*. (B) Walker A motif (in red, residues characterizing the motif; *A. thaliana* NADKc amino acids 236-250). For gene references, see the legend of Fig. S6.



**Figure S3**

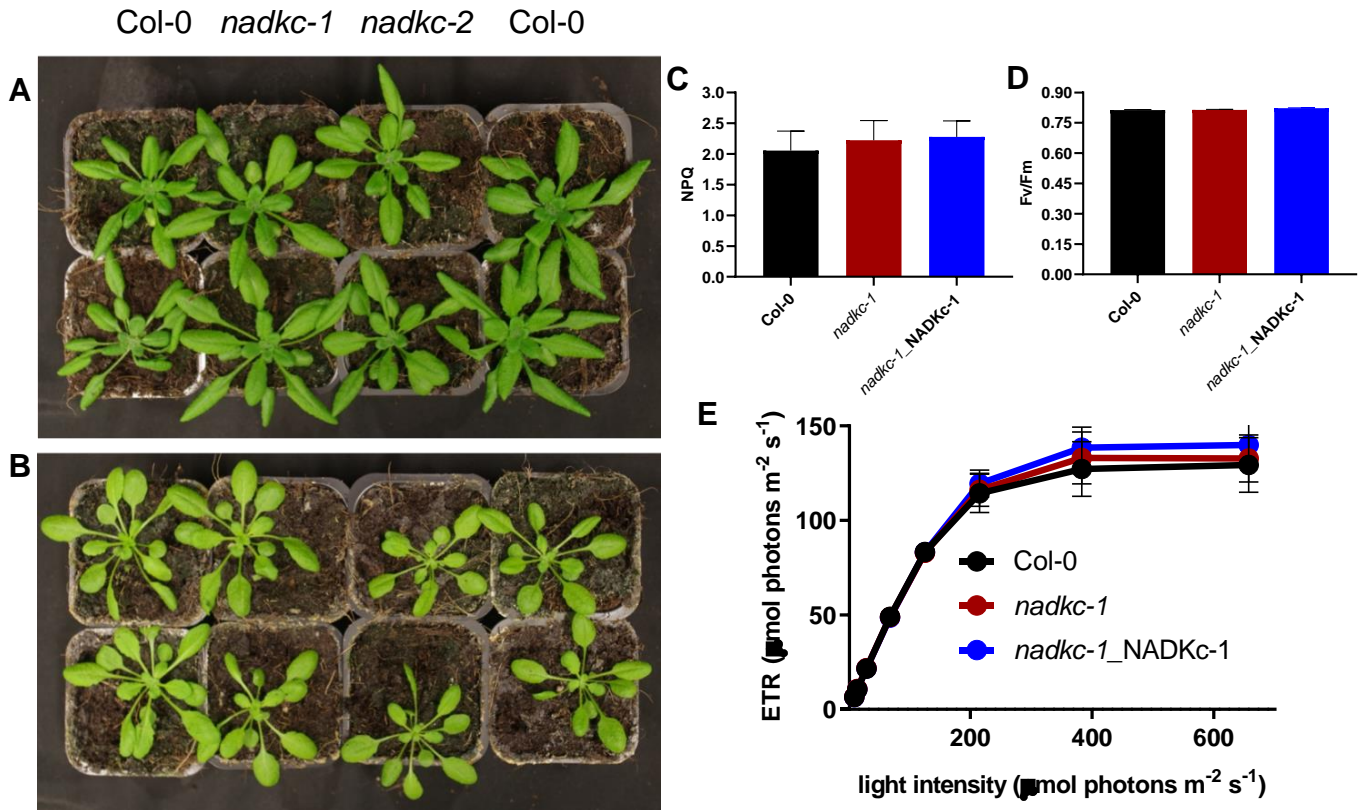


**Supplemental Figure S3.** Purification of recombinant NADKc produced in *E. coli*. 6HIS-Δ38NADKc was purified as indicated in Material and Methods. Lane 1: Rosetta2 soluble extract transformed with empty pET28a (40 μg); lane 2: Rosetta2 soluble extract transformed with pET28a6HIS-Δ38NADKc (40 μg); lane 3: Ni-NTA pool (10 μg); lane 4: urea-denatured 6HIS-Δ38NADKc purified on Ni-NTA (10 μg); lane 5: refolded 6HIS-Δ38NADKc (2 μg).

**Figure S4**

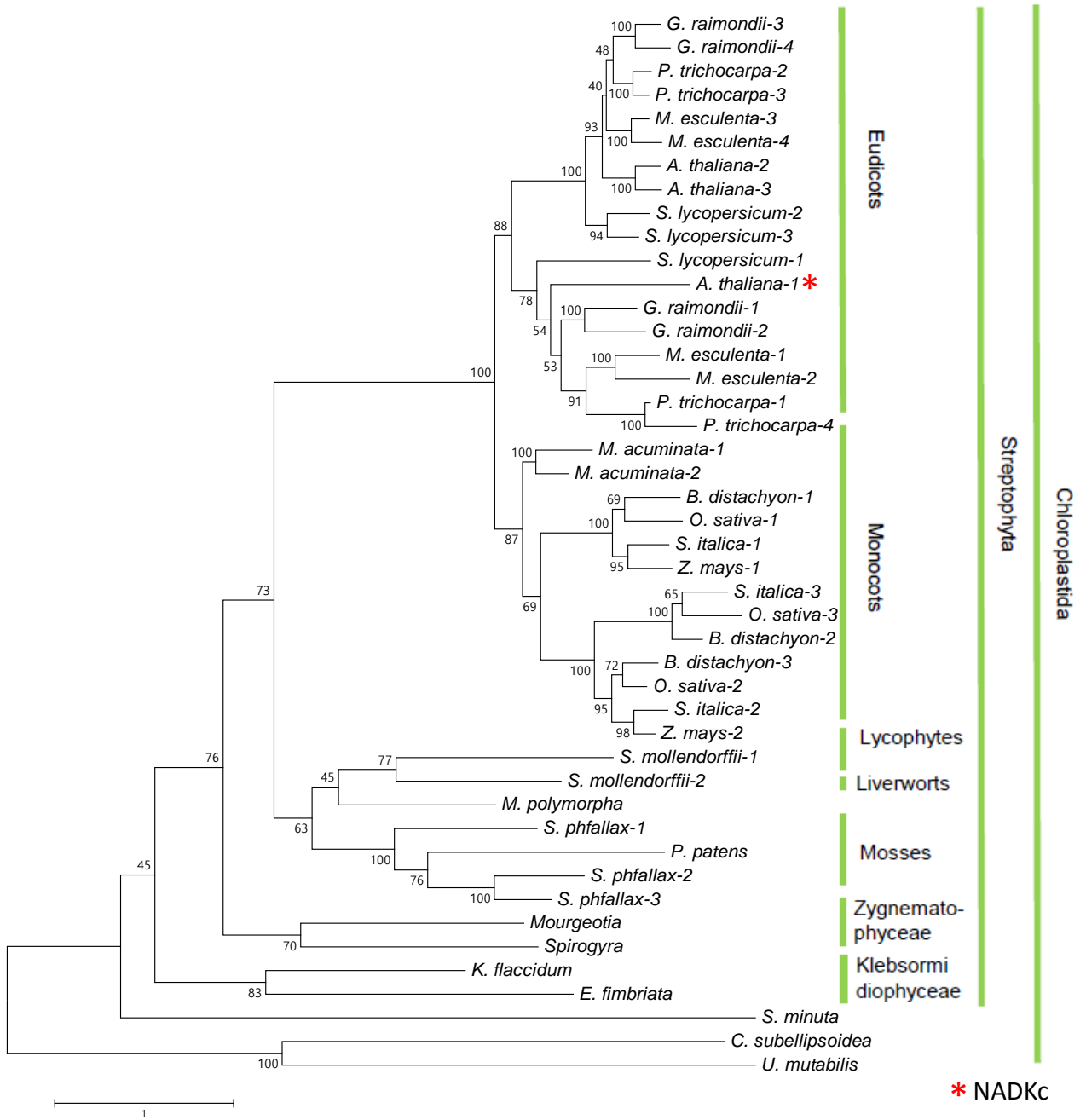
**Supplemental Figure S4. A.** NADKc<sub>Nter</sub>-YFP associates with mitochondria in *N. benthamiana* leaves. Representative pictures of transiently transformed *N. benthamiana* leaf cells. Left: YFP (green), Center: RFP (red), and Right: merged fluorescence. The top row shows a representative image of *N. benthamiana* cells co-transformed with the NADKc<sub>Nter</sub>-YFP construct and a mitochondrial marker, pSu9-RFP. The second row shows a close-up of mitochondria from the lower right region of the images in the top row (white boxes). White arrows indicate regions in which the YFP signal appears peripheral with respect to the RFP signal. The third row shows a representative image of *N. benthamiana* cells transformed with the YFP-NADKc construct alone. The central image shows the background signal in the RFP channel. White bars represent 2  $\mu$ m in the first and second row, and 10  $\mu$ m in the third row. **B.** Full length NADKc-YFP stably expressed in *Arabidopsis* forms aggregates in the cytosol. White bars represent 5  $\mu$ m.

**Figure S5**



**Supplemental Figure S5.** Phenotype of *nadkc* mutants. (A) 21-day-old plants grown under long day photoperiod (16 h light/8 h dark); (B) 28-day-old plants grown under short day photoperiod (8 h light/16 h dark). (C-E) Photosynthetic parameters in Col-0 and *nadkc* plants: (C) NPQ, (D) Fv/Fm and (E) electron transport rate.

Figure S6



**Supplementary Fig. S6.** Phylogeny of NADKc. Maximum likelihood phylogenetic tree of NADKc-like proteins in the following plant and algal species: *Arabidopsis thaliana* (*A. thaliana*), *Populus trichocarpa* (*P. trichocarpa*), *Manihot esculenta* (*M. esculenta*), *Gossypium raimondii* (*G. raimondii*), *Solanum lycopersicum* (*S. lycopersicum*), *Setaria italica* (*S. italica*), *Zea mays* (*Z. mays*), *Oryza sativa* (*O. sativa*), *Brachypodium distachyon* (*B. distachyon*), *Musa acuminata* (*M. acuminata*), *Marchantia polymorpha* (*M. polymorpha*), *Physcomitrella patens* (*P. patens*), *Sphagnum phallax* (*S. phallax*), *Selaginella mollendorffii* (*S. mollendorffii*), *Klebsormidium flaccidum* (*K. flaccidum*), *Coccomyxa subellipsoidea* (*C. subellipsoidea*), *Ulva mutabilis* (*U. mutabilis*), *Spirotaenia minuta* (*S. minuta*), *Mougeotia* sp., *Spirogyra* sp. and *Entransia fimbriata* (*E. fimbriata*). Accession numbers: *A. thaliana*-1 (NADKc): At1g04280, *A. thaliana*-2: At1g06750, *A. thaliana*-3: At2g30630, *P. trichocarpa*-1: Potri.008G162000, *P. trichocarpa*-2: Potri.002G043000, *P. trichocarpa*-3: Potri.005G220000, *P. trichocarpa*-4: Potri.008G162400, *M. esculenta*-1: Manes.15G036900, *M. esculenta*-2: Manes.03G168900, *M. esculenta*-3: Manes.01G200600, *M. esculenta*-4: Manes.05G086200, *G. raimondii*-1: Gorai.011G171100, *G. raimondii*-2: Gorai.006G246600, *G. raimondii*-3: Gorai.004G074100, *G. raimondii*-4: Gorai.013G104300, *S. lycopersicum*-1: Solyc06g053810, *S. lycopersicum*-2: Solyc06g031670, *S. lycopersicum*-3: Solyc08g059750, *S. italica*-1: Seita.9G163700, *S. italica*-2: Seita.3G185100, *S. italica*-3: Seita.5G337000, *Z. mays*-1: GRMZM2G070252, *Z. mays*-2: GRMZM2G368410, *O. sativa*-1: Os03g43010, *O. sativa*-2: Os05g43300, *O. sativa*-3: Os01g56764, *B. distachyon*-1: Bradi1g14307, *B. distachyon*-2: Bradi2g51490, *B. distachyon*-3: Bradi2g20400, *M. acuminata*-1: SMUA\_Achr5T03210, *M. acuminata*-2: GSMUA\_Achr7T01560, *M. polymorpha*: Mapoly0142s0012, *P. patens*: Pp3c2\_3490V3, *S. phallax*-1: Sphallax0059s0037, *S. phallax*-2: Sphallax0011s0002, *S. phallax*-3: Sphallax0120s0019, *S. mollendorffii*-1: scaffold 73427, *S. mollendorffii*-2: scaffold 231175, *K. flaccidum*: kfl00274\_0130, *C. subellipsoidea*: XP\_005648203, *U. mutabilis*: UM028\_0076.1, *S. minuta*: NNHQ\_2000691, *Mougeotia*: ZRMT\_2002068, *Spirogyra*: HAOX\_2025158, *E. fimbriata*: BFIK\_2025349. The tree is drawn to scale, with branch lengths measured in the number of substitutions per site (scale bar in the bottom-left corner). The numbers at the interior nodes are bootstrap percentages.



## Table S2: Primers used in this study

In red: sequences for recombination reactions by BP clonase into pDONR221.

Uppercase: restriction enzyme sites.

### Primers for cloning the NADKc protein sequence for enzymatic, localization and complementation studies:

construct	Forward primer	Reverse primer
pet28(b)-6-HIS-NADKc	gacttttcaaaccacCATATGgtgaaac ccttaggagaag	caaattcaggaagaagaCTCGAGcaaagg tctagttc
pet28(b)-6-HIS-D38NADKc	gctgtagcagctCATATGgccggagaat tactc	caaattcaggaagaagaCTCGAGcaaagg tctagttc
35S::NADKc <sub>Nter</sub> -YFP (in pB7YWG2,0)	<b>GGGGACAAGTTTGTACAAAAAGCAGGC</b> <b>T</b> Tgatggtgaaacccttaggagaag	<b>GGGGACCACTTTGTACAAGAAAGCTGGGT</b> ggacatctttatacccccattg
35S::NADKc-YFP (in pB7YWG2,0)	<b>GGGGACAAGTTTGTACAAAAAGCAGGC</b> <b>T</b> Tgatggtgaaacccttaggagaag	<b>GGGGACCACTTTGTACAAGAAAGCTGGGT</b> atTTTTTggttgggccttttcgattctcc
35S::YFP-NADKc (in pB7WGY2,0) and 35S::NADKc (in pB2GW7,0)	<b>GGGGACAAGTTTGTACAAAAAGCAGGC</b> <b>T</b> Tgatggtgaaacccttaggagaag	<b>GGGGACCACTTTGTACAAGAAAGCTGGGT</b> tcaatTTTTTggttgggccttttcgattctcc

### Primers for genotyping:

line	Forward primer	Reverse primer	LB primer
SALK_130871	tgtaagcaaatatgtg ggcc	acaaatgatcgaaatgg caag	LBb1.3 atTTTgcccattttcgg aac
GABI_311H11	taaggaagaaggacggg acttc	tcaagatcgaccaaagc attag	LBgabi-kat atattgaccatcatact cattgc

### Primers for gene expression studies (qPCR):

	Forward primer	Reverse primer
At1g04280	aacgggtcagcagtcctcaa c	gggcctcgatggaactaac a